Theoretical and Applied Climatology (2024) 155:7609–7628
https://doi.org/10.1007/s00704-024-05034-1

RESEARCH

Carbon and water vapor exchanges coupling for different irrigated and rainfed conditions on Andean potato agroecosystems

Fabio Ernesto Martínez-Maldonado[1,2,3,4] · **Angela María Castaño-Marín**[2] · **Gerardo Antonio Góez-Vinasco**[3] · **Fabio Ricardo Marin**[4]

Received: 18 October 2023 / Accepted: 16 May 2024 / Published online: 3 July 2024

Abstract

The fundamental exchange of water for carbon lays the groundwork for understanding the interplay between carbon and water cycles in terrestrial ecosystems, providing valuable insights into global water and carbon balances and vegetation growth. Inherent water use efficiency (IWUE) was used as a study framework of the diurnal patterns and degree of coupling of carbon and water exchange to investigate the net ecosystem carbon exchange (NEE) responses of three water regime potato cropping systems [full-irrigation (FI), deficit-irrigation (DI), and rainfed (RF)] in Cundinamarca, Colombia. The eddy covariance method was used to determine CO_2 and water fluxes, surface resistances, and the omega decoupling factor (Ω). Additionally, leaf area index (LAI), and specific leaf area (SLA) were assessed to determine the canopy influence on carbon and water exchange. The highest carbon sink activity (NEE = -311.96 ± 12.82 g C m^{-2}) at FI, is primarily attributed to a larger canopy with high autotrophic activity and low internal resistance. This supported a highly coupled and synchronized exchange between evapotranspiration (ET) and gross primary production (GPP), as reflected in the highest IWUE (4.7 mg C kPa s^{-1} kg^{-1} H_2O). In contrast, the lower sink capacity at DI (NEE = − 17.3 ± 4.6 g C m^{-2}) and the net carbon source activity from RF (NEE = 187.21 ± 3.84 g C m^{-2}) were related to a smaller leaf area available for water and carbon exchange, resulting in lower IWUE (2.3 and 1.01 mg C kPa s^{-1} kg^{-1} H_2O, respectively) and a decoupled and desynchronized gas exchange caused by unbalanced restrictions on ET and GPP fluxes. These results provide new information on carbon–water interactions in potatoes and improve the understanding of carbon sequestration and drought effects on potato sink activity.

1 Introduction

Vegetation plays a crucial role in achieving carbon neutrality through photosynthetic CO_2 sequestration (Guo et al. 2017; Liu et al. 2021). Therefore, it is important to understand how agroecosystems can act as carbon sinks and reduce the carbon flux from land to the atmosphere (Wood 2021). Net ecosystem carbon exchange (NEE), calculated as the difference between Ecosystem respiration (R_{eco}) and Gross primary production (GPP), reflects the amount of CO_2 captured or emitted by vegetation (Liu et al. 2021). It provides a means to identify and monitor carbon sinks and sources (Fei et al. 2017; Wood 2021). It is important to note that all CO_2 captured by vegetation during photosynthesis is inherently associated with water loss (Field et al. 1995; Tang et al. 2015). In this regard, plants tend to optimize the increase in carbon gain (GPP) while minimizing water losses (ET) (Katul et al. 2009, 2010). This results in a negative NEE and a net gain of CO_2 for the ecosystem (Scott et al. 2006; Díaz et al. 2022). However, under drought conditions, the availability of water to support GPP is limited, and the rate of carbon uptake decreases (Law et al. 2000; Reichstein et al. 2002; Ciais et al. 2005; Pereira et al. 2007; Schwalm et al. 2010; Zhou et al. 2013). Consequently, NEE shifts from uptake to emission of carbon (Ciais et al. 2005; Jongen

✉ Fabio Ernesto Martínez-Maldonado
femartinez@agrosavia.co

1 Corporación Colombiana de Investigación Agropecuaria—Agrosavia, Centro de Investigación Tibaitatá, Km 14 Vía Mosquera , 250047 Cundinamarca, Bogotá, Colombia

2 Corporación Colombiana de Investigación Agropecuaria—Agrosavia, Centro de Investigación La Selva, Km. 7, Vía Rionegro - Las Palmas, Sector Llanogrande, 054048 Antioquia, Rionegro, Colombia

3 Grupo de Investigación de Agua y Saneamiento, Universidad Tecnológica de Pereira—UTP, 660003 Pereira, Colombia

4 Luiz de Queiroz" College of Agriculture, University of São Paulo, Piracicaba, SP 13418-900, Brazil

et al. 2011), potentially diminishing the crop's capacity to function as carbon sink (Jongen et al. 2011).

Water and carbon fluxes are tightly coupled systems (Brunsell and Wilson 2013; Gentine et al. 2019; Van Dijke et al. 2020; Díaz et al. 2022) and tend to be synchronized because they share common environmental controls and the stomatal pathway for water vapor and CO_2 exchange during photosynthesis (Leuning 1995; Lombardozzi et al. 2012; Lin et al. 2015; Gentine et al. 2019; Krich et al. 2022). This critical tradeoff between water (ET) and carbon (GPP) fluxes (Law et al. 2002; Díaz et al. 2022) can be quantitatively assessed through water use efficiency (WUE). WUE serves as a link between water and carbon fluxes, acting as a key indicator of CO_2-water coupling within ecosystems (Hu et al. 2008; Niu et al. 2011; Keenan et al. 2013; Tang et al. 2015; Ali et al. 2017; Gentine et al. 2019; Li et al. 2022). Nevertheless, while the WUE concept provides essential insights for optimizing water and carbon management in crop production (Keenan et al. 2013; Xie et al. 2016; Oo et al. 2023), it is important to acknowledge that the effect of vapor pressure deficit (VPD) on canopy conductance can lead to misinterpretation of carbon uptake and water loss responses to environmental conditions (Wagle et al. 2016).

Several studies have indicated that WUE strongly depends on VPD at daily or hourly time scales (Morén et al. 2001; Herbst et al. 2002; Abbate et al. 2004; Tang et al. 2006; Hu et al. 2008; Beer et al. 2009; Linderson et al. 2012; Zhou et al. 2014, 2015). Hence, the alternative concept of Inherent Water Use Efficiency (IWUE) was proposed to include the effects of VPD on the photosynthesis–transpiration relationship through stomatal conductance (Bierhuizen and Slatyer 1965; Beer et al. 2009; Launiainen et al. 2011; Zhou et al. 2014, 2015). This approach is analogous to leaf-level intrinsic water-use efficiency (iWUE), defined as the ratio of net photosynthesis fluxes to water vapor conductance (Beer et al. 2009; Li et al. 2017). At the ecosystem scale, IWUE = (GPP*VPD)/ET can be calculated utilizing measurements of carbon (GPP) and water (ET) fluxes acquired via the eddy covariance method. This approach is based on the premise that carbon assimilation is proportional to GPP, while VPD/ET serves as a proxy for canopy conductance (Beer et al. 2009). Derived from IWUE, the robust linear correlation between GPP*VPD and ET(Beer et al. 2009) has been extensively employed to compare diurnal cycles of carbon and water fluxes (Nelson et al. 2018) and to investigate the interactions between carbon and water dynamics (Loader et al. 2011; Leonardi et al. 2012; Battipaglia et al. 2013; Grossiord et al. 2014; Zhou et al. 2014). IWUE represents the intrinsic link between carbon and water fluxes via stomatal conductance. Yet, the extent of surface control by stomata depends on the degree of decoupling [omega coefficient, (Jarvis and Mcnaughton 1986)] between the plant canopy and the atmosphere (Steduto and Hsiao 1998), a relationship further affected by VPD and soil water availability. Consequently, incorporating the impact of VPD yields a more physiologically insightful approach for studying carbon–water interactions.

Potato represents the world's foremost non-grain crop, and with its extensive cultivation area (more than 19 million hectares), it is an important agroecosystem for global carbon and greenhouse gas balances (Devaux et al. 2014). However, despite the growing interest in studying the carbon balance of potatoes, there is no consensus on the carbon sink potential due to the wide variability in cultivars and crop management practices (Aubinet et al. 2009; Moors et al. 2010; Waldo et al. 2016; Buysse et al. 2017; Meshalkina et al. 2017, 2018). To our knowledge, there has been a lack of research into the mechanisms and interactions between carbon and water coupling and their association with NEE in potato agroecosystems. Specifically, studies investigating how water availability modulates the carbon sink or source dynamics of potato, based on the water-carbon tradeoff, have yet to be conducted. The available studies on sink capacity have focused on the effect of climate or management on carbon fluxes (NEE, GPP, R_{eco}) independently of water vapor flux (ET) (Aubinet et al. 2009; Moors et al. 2010; Buysse et al. 2017; Meshalkina et al. 2017, 2018), and were conducted for "European" potatoes (*S. tuberosum* Chilotanum Group). However, approximately half of the global potato harvest comes from developing countries (Birch et al. 2012; Hill et al. 2021), where "Andean" potatoes, *S. tuberosum* Andigenum Group (Raker et al. 2002; Ghislain et al. 2009) serve as a primary source of income (Mosquera Vásquez et al. 2017; Hill et al. 2021) and are cultivated in tropical highlands under both industrial irrigated fields and rainfed systems. We hypothesize that under well-watered conditions, a robust coupling between GPP and ET fluxes leads to elevated IWUE and, consequently, enhanced diurnal sink activity (more negative NEE). In rainfed systems, severe drought episodes may compromise the carbon sink capacity of potatoes, attributable to the decoupling of carbon and water fluxes and the asynchronous response of GPP and ET. This study details the responses of the net ecosystem carbon exchange (NEE) to variations in water availability conditions, elucidating the dynamics of H_2O and CO_2 exchanges between the canopy and atmosphere across three distinct potato cropping systems subjected to different water regimes. Carbon and water flux measurements were utilized from three predominant potato production models in the major potato-producing region of Colombia; two different irrigated potato fields and one rainfed system to achieve the following objectives: (a) quantify the magnitudes of net ecosystem CO_2 exchange (NEE) and its components (gross primary production, GPP, and ecosystem respiration, R_{eco}) in irrigated and rainfed potato

crops, (b) investigate the impact of water deficit periods on carbon and water vapor fluxes and explore the role of leaf area in controlling these fluxes, and (c) study and quantify the ET-GPP coupling and inherent water use efficiency (IWUE) in irrigated and rainfed potato crops.

2 Methods

2.1 Site description

The study area is located in a fluvio-lacustrine plain, a landscape that emerged from the silting of an ancient lake which once filled various tectonic depressions created during the uplift of the eastern mountain range. The soils are significantly influenced by volcanic ash from the volcanic formations of the central mountain range and are primarily characterized as belonging to the Andisol, Inceptisol and Vertisol orders (Soil Survey Staff 2014). The soils of the terrace relief generally have a depth greater than one meter, however, in the decaying marshes and valleys reliefs, the shallow soils are limited by the water table. The average annual temperature varies between 12 and 14 °C, while annual rainfall amounts range from 500 to 1000 mm distributed bimodally. The June—August and December—February periods are the ones with the lowest rainfall (Martínez-Maldonado et al. 2021).

The full-irrigation (FI) cycle was implemented on a 3.11-hectare commercial plot in the Municipality of Subachoque, situated within Cundinamarca, Colombia. This location, defined by the coordinates 4°53′19" N and 74°11′12" W, is elevated at 2609 m above sea level. Irrigation scheduling involved assessing the water needs of the potato crop at each stage of the growing season in conjunction with monitoring soil water status and meteorological conditions. A fixed sprinkler irrigation system operating at 3 bar with a flow rate of 1.03 m^3/h was used because of its ability to provide uniform water application throughout the growing season. Sprinklers were installed at 10 m x 10 m spacing, based on the average radius of the emitter's wetting diameter. The overall irrigation efficiency was estimated at 85%, considering factors such as uniformity of water distribution and losses due to evaporation and wind drift in the Subachoque region. Temperature, relative humidity, and wind speed measured via the Eddy covariance tower were variables used in calculating the reference evapotranspiration (ETo) to adjust irrigation scheduling and meet the specific needs of the crop at different stages of its development according to the crop coefficient (Kc) for potatoes (FAO 56). Adjustments were made based on tensiometer readings and monitoring of the soil's water status to optimize water application without exceeding field capacity or reaching the permanent wilting point. The Deficit-irrigation (DI) cycle was conducted on a commercial lot spanning 9.5 hectares located in the municipality of Facatativá, Cundinamarca, Colombia (4°48′13" N, 74°17′20" W, approximately 2573 m above sea level). In this instance, the farmer scheduled a weekly application of a 20 mm water layer using a cannon irrigation system, exclusively during periods when the crop development was most susceptible to water stress, specifically during the vegetative growth and tuberization stages. This scheduling was performed without an analysis of the soil's water status, meteorological conditions, or the specific needs of the crop at its respective developmental stage. This resulted in a less efficient water management strategy. The rainfed (RF) cycle was carried out in a 3-hectare lot located in the municipality of Tenjo, Cundinamarca, Colombia (4°52′13.188" N, 74°7′45.84" W, approximately 2572 m above sea level).

The potato (*Solanum tuberosum* L.) variety Diacol Capiro was planted across the three study plots at a plant density of 33,333 pl ha^{-1}. The planting dates were January 22, 2021, for the FI cycle, February 27, 2020, for the DI cycle and August 1, 2020, for the RF cycle. In the three farming configurations (Full-irrigation, Deficit-irrigation, and Rainfed), farmers implemented typical agronomic practices recommended for potato cultivation in the Cundinamarca region. The fertilizer application routine of farmers across the three subregions of Cundinamarca involved the application of 120 kg ha^{-1} of nitrogen, 80–100 kg ha^{-1} of P_2O_5, and 150 kg ha^{-1} of K_2O to the soil prior to planting. The fertilizers utilized by farmers include slow-release urea, triple superphosphate and balanced fertilizers in a ratio of 10:30:10:5, 14:3:18:8:0:7 and 12:11:18:0:2:2,7:8 of N, P, K, Ca, Mg, S, Zn, B, and Cu. The planting was conducted using vegetative seed, followed by an initial phosphate-rich soil fertilization. During the tuber bulking phase, foliar fertilization was carried out with 30 kg ha^{-1} of nitrogen, 50 kg ha^{-1} of potassium, and a complex of essential micronutrients. The dosages of these nutrients are adjusted based on soil analysis for each potato plot before the campaign. For weed control, pre-emergent and post-emergent herbicides were applied. Hilling, which involves piling soil around the plants, was carried out several weeks after seedling emergence to help protect the developing tubers from direct sunlight and to promote better development. For pest and disease management, regular control measures were implemented using insecticide and fungicide treatments upon the first signs of infestation. Close to harvest, chemical dehaulming was performed to strengthen the potato skins, followed by harvesting when the tubers were fully mature and soil conditions were optimal. The Full-Irrigation plot exhibits a loam texture (F) with 17.0% organic matter, a volumetric field capacity of 47%, a volumetric permanent wilting point of 35.0% (PWP at 15 bar), and an apparent density 0.66 g cm^{-3}. The Rainfed plot also has a loam texture (F), but with 22.0%

organic matter, a volumetric field capacity of 40%, a volumetric permanent wilting point of 28.0% (PWP at 15 bar), and an apparent density 0.60 g cm^{-3}. The Deficit-Irrigation plot features a silty loam texture (L-F) with 13.0% organic matter, a volumetric field capacity of 49.0%, a volumetric permanent wilting point of 36.0% (PWP at 15 bar), and an apparent density 0.60 g cm^{-3}.

2.2 Eddy covariance and soil measurements

Net carbon exchange and weather variables within the experimental fields were continuously monitored using an Eddy Covariance (EC) station. In the DI site, the station was installed on March 19, 2020; in the RF site on August 13, 2020; and in the FI site on February 03, 2021. The measurements reported in this study span from March 19, 2020 to July 30, 2020 for DI cycle, from August 11 to December 11, 2020 for RF cycle, and from February 02 until June 07, 2021 for FI cycle. The setup of the Eddy Covariance (EC) micrometeorological station deployed at each evaluation site included both primary and supplementary sensors. The EC tower was equipped with an IRGASON open-path gas analyzer (EC 150, Campbell Scientific, Inc., Logan, UT, USA) and a 3D sonic anemometer (CSAT3A, Campbell Scientific, Inc., Logan, UT, USA), both of which were managed by a separated electronic module (EC100, Campbell Scientific, Inc., Logan, UT, USA). Raw data were captured at a sampling frequency of 10 Hz using a high-performance datalogger (CR1000X, Campbell Scientific, Inc., Logan, UT, USA). The tower height for the study sites was determined using the formula $hEC = Zd + 4\ (hc - Zd)$ (Foken et al. 2012), where, hEC = EC installation height, Zd = zero plane displacement (0.63 m) and hc = average height of the crop (0.9 m). The IRGASON was placed at a 1.7 m height. The IRGASON's azimuth was set to 45° for the Rainfed (RF) cycle, 315° for the Deficit-Irrigation (DI) cycle, and 175° for the Full-Irrigation (FI) cycle. These orientations corresponded to the prevailing wind directions as recorded by the sonic anemometer three weeks prior to the commencement of the evaluations. Additional sensors installed included: a Net Radiometer (NR-LITE2, Kipp & Zonen B.V., Delft, The Netherlands) at 2 m height to measure incoming and outgoing short-wave and long-wave radiation (Rn); three Photosynthetically Active Radiation (PAR) sensors (CS310, Apogee Instruments, Inc., Logan, UT, USA) positioned at heights of 0.5, 1, and 2.2 m; a pyranometer sensor (CS301, Apogee Instruments, Inc., Logan, UT, USA) at 2 m height for measuring total incident radiation; and two air temperature (Tair) and relative humidity sensors (HygroVUE™ 10, Campbell Scientific, Inc., Logan, UT, USA) installed at heights of 1 and 2 m, respectively. Climatic data were recorded at 5-min intervals, with averages subsequently integrated on a half-hourly basis. Precipitation data were collected daily using a rain gauge connected to a datalogger (Oregon Scientific, Inc., Tualatin, OR, USA) positioned at a height of 2 m. Soil heat flux density (G, in W/m^2) was determined by averaging the measurements from two HFP01 sensors (Hukseflux Thermal Sensors B.V., Delftechpark, Delft, The Netherlands), which were installed 88 cm apart at a depth of 8 cm. Two multiparameter smart sensors (CS655, Campbell Scientific, Inc., Logan, UT, USA) were employed to monitor soil volumetric water content (SWC) at a depth of 20 cm, bulk electrical conductivity, and soil temperature. Additionally, four type E thermocouples (TCAV-Averaging Soil Thermocouple Probe, Campbell Scientific, Inc., Logan, UT, USA) were installed, with each pair positioned at depths of 8 cm and 15 cm, respectively. This installation aligns with the manufacturer's recommendation to accurately capture soil temperature within the active root zone, which is typically between 5 and 20 cm depth. The volumetric soil water content (SWC) sensor was previously calibrated to match the site-specific conditions. This calibration process adhered to the manufacturer's guidelines as detailed in Campbell Scientific's documentation (Campbell Scientific 2020) and involved collecting soil samples in triplicate. Approximately 25 kg of soil from the study area was collected and air-dried. This dried soil was then placed into containers with a diameter of 20 cm and an effective depth of 24 cm, preserving the bulk density noted in the field. The sensor measured dielectric permittivity, and soil subsamples were taken in triplicate to determine moisture content via oven drying. Subsequently, the soil sample was subjected to successive cycles of wetting and homogenization. A total of six calibration points were recorded for each set of repetitions, spanning moisture levels from 10 to 50%.

For the data processing and quality assurance of the Eddy Covariance system, raw data time series were captured at a frequency of 10 Hz. Latent and sensible heat, as well as CO_2 fluxes were computed at half-hour intervals utilizing the EasyFlux® CRBasic software suite (Campbell Scientific, Inc., Logan, UT, USA), which was configured on the CR1000X datalogger. The data underwent several correction procedures, including despiking, filtering of high-frequency time series data, coordinate rotation employing the planar fit method, frequency adjustments based on co-spectral analysis, and air density fluctuation corrections. Additionally, data quality was assessed through classifications (QC) and footprint characteristic computations. Advanced post-processing of the flux data included applying fetch filters, detecting, and eliminating outliers, and implementing a QC filter. Gap-filling for both Eddy Covariance and associated meteorological data was executed in R, taking into account the co-variation between the fluxes and meteorological variables, alongside their temporal autocorrelations (Martínez-Maldonado et al. 2021).

2.3 NEE partitioning between gross primary productivity GPP and ecosystem respiration R_{eco}

The exponential Mitscherlich light-response function, was employed to partition diurnal NEE (when solar global radiation > 1 W m^{-2}) into ecosystem respiration (R_{eco}) and GPP (Falge et al. 2001; Tagesson et al. 2015):

$$NEE = -\left(A_{gmax} + R_d\right) * \left(1 - \exp^{\left(\frac{-\Phi * I_{inc}}{A_{gmax}+R_d}\right)}\right) + R_d \quad (1)$$

where Ag_{max} is the light saturated CO_2 uptake [μ_{mol} (CO_2) m^{-2} s^{-1}]; R_d is respiration [μ_{mol} (CO_2) m^{-2} s^{-1}], ϕ is the quantum yield [μ_{mol} (CO_2) μ_{mol} (photon) $^{-1}$], and I_{inc} is the incident PPFD [μ_{mol} (photon) m^{-2} s^{-1}]. Calculations, data post-processing, quality control, gap-filling, energy balance closure, uncertainty and statistical analysis methods are described in (Martínez-Maldonado et al. 2021).

2.4 ET-GPP coupling analysis

2.4.1 Inherent water use efficiency

The IWUE was assessed at both, daily and half hour temporal scales following the theoretical framework proposed by (Beer et al. 2009). This approach is rooted in the intrinsic water-use efficiency (iWUE) concept, which is defined as the ratio of the fluxes of net photosynthesis (A) and conductance for water vapor (g_{H_2Ov}) (Leonardi et al. 2012):

$$Being\ A = g * (\Delta c) \quad (2)$$

$$And\ E = (1.6 * g) * (\Delta v) \quad (3)$$

$$then,\ iWUE = \frac{A}{g_{H_2Ov}} = \frac{g * (\Delta c)}{1.6 * g} = \frac{\Delta c}{1.6} \quad (4)$$

where Δc and Δv are the difference between ambient and inner leaf partial pressure of CO_2 y and H_2O_v pressure, respectively; *g* is stomatal conductance; 1.6 is the molar diffusivity ratio of CO_2—H_2O (i.e., $gH_2O = gCO_2 * 1.6$, lighter H_2O molecules diffuse more rapidly than CO_2); "1.6*g" is the stomatal conductance for water vapor (Gentilesca et al. 2021). Approximating the vapor pressure difference Δ*v* by atmospheric VPD, leaf net photosynthesis A and transpiration E by GPP and ET fluxes respectively, inferred from eddy covariance observations, and g_{H_2Ov} by *g'* as the conductance at the ecosystem level proposed by Beer et al. (2009), Eq. (3) is solved as:

$$g' = \frac{ET}{1.6 * VPD} \quad (5)$$

The inherent water use efficiency (IWUE) is then represented by:

$$IWUE = \frac{GPP}{g'} = \frac{g' * (\Delta c')}{1.6 * g'} = \frac{\Delta c'}{1.6} = \frac{GPP}{1.6 * \left[\frac{ET}{1.6 * VPD}\right]} = \frac{GPP * DPV}{ET} \quad (6)$$

where GPP is the Gross Primary Productivity [μ_{mol} (CO_2) m^{-2} s^{-1}]; *g* is the stomatal conductance at the ecosystem level [mol (H_2O) m^{-2} s^{-1}]; Δc is the gradient of CO_2 concentration inside and outside the leaf at the ecosystem level (μmol mol^{-1}); ET is the actual evapotranspiration (mm H_2O d^{-1}); VPD is a vapor pressure deficit (kPa). The usage of marker ' indicates that variables are analyzed at ecosystem level.

2.4.2 Diurnal and daily ET-GPP coupling and synchrony

Equation 6 reveals a linear relationship between GPP and ET, which is adjusted by VPD. To quantify the degree of carbon–water coupling for each day, the linear correlation coefficient between ET and GPP*VPD was computed using half-hourly data (Zhou et al. 2014; Nelson et al. 2018; Aguilos et al. 2021). These correlation coefficients were determined at both, the daily scale for the entire crop growth period at each site, and the average half-hourly scale for each growth stage (vegetative, tuberization and tuber bulking) at each site. When correlation values approach unity (r > 0.85), it suggests strong coupling and synchronization between the two fluxes. Conversely, low correlation values indicate carbon–water decoupling and a poor synchronization of the fluxes (Nelson et al. 2018).

2.4.3 Coupling between the plant canopy and the atmosphere

The degree to which stomatal and canopy conductance influence water vapor and CO_2 exchange was evaluated using the decoupling factor omega (Ω), calculated at the daily scale using the formulation proposed by Jarvis and Mcnaughton (1986):

$$\Omega = \frac{1}{1 + \left[\left(\frac{2Rc}{\left(\frac{s}{\Upsilon}+2\right)}\right)\right] * Ra} \quad (7)$$

where *Ra* is the aerodynamic resistance of the canopy (s m^{-1}); *Rc* is the canopy stomatal resistance to vapor diffusion (s m^{-1}); and ϒ is the psychrometric constant (kPa $°C^{-1}$). The *Rc* was computed at both daily and half-hourly temporal scales using:

$$Rc = \frac{\rho * cp * VPD}{\Upsilon * LE} + \left(\frac{\Delta}{\Upsilon}\beta - 1\right) * Ra \quad (8)$$

where ρ is the mean air density (kg m^{-3}); cp is the specific heat of air at constant pressure (J kg^{-1} K^{-1}), Δ is the slope of the saturation vapor pressure–temperature curve calculated at the air temperature T_a (kPa $°C^{-1}$); β is the Bowen ratio (dimensionless) and Ra is the aerodynamic resistance. Finally, Ra was calculated for both, daily and half-hourly temporal scales by:

$$Ra = \frac{ln\left(\frac{Z}{Zo_v}\right)}{u^* K^2} \quad (9)$$

where k is the von Karman constant (dimensionless, approximately 0.41); $u*$ is the friction velocity (m s^{-1}), z is the measurement height (m); and z_{ov} is the surface roughness for water vapor, a fraction of the canopy height h (m) typically around 0.01 time h.

2.5 Biological measurements and growth analysis

From planting and throughout crop growth, plant sampling via sequential harvesting was conducted. Every 11 or 12 days, ten plants were randomly uprooted for growth analysis after 35, 41, 48, 57, 63, 69, 78, 84, 97, 104, 112, 124, 133, and 147 days post planting (DPP) at DI site; after 25, 37, 47, 54, 65, 75, 85, 98, 105, and 116 DPP at RF site and 33, 46, 57, 70, 80, 96, 110, 122, 135 and 152 DPP, at FI site. The plants were divided into four components: green leaves (lamina and petiole), roots, stems, and tubers. The total leaf area of each sample was determined by using an image processing algorithm from green leaves RGB images. Subsequently, plant material was placed in paper bags and dried in a forced-air drying oven until a constant weight was achieved at 70 °C. Dry weight data for leaves, roots, stems, and tubers (obtained using an electronic scale A&D Weighing, 0.1 g) were fitted to nonlinear functions.

Growth and morphological parameters such as specific leaf area (SLA) and leaf area index (LAI) were calculated as outlined by Hunt (1990).

$$LAI = \frac{LA}{P} \quad (10)$$

where LA is total leaf area per plant (m^{-2}) and P denotes the unit of land area (m^{-2}). The SLA quantifies the density or relative thinness of leaves, which relates the leaves area to their dry weight (Hunt 1990):

$$SLA = \frac{\left[\left(\frac{LA_1}{LW_1}\right) + \left(\frac{LA_2}{LW_2}\right)\right]}{2} \quad (11)$$

where LW is total leaf dry weight per plant (g).

LAI and SLA were fitted to the logistic growth model $f(t) = A/1 + be^{-(ct)}$ where, "A" is the maximum value reached by the variable, "c" is the product of the initial value "ai" and maximum "A" and "b" is the rate of growth.

3 Results

3.1 Meteorological conditions

The average of daily mean PPFD was observed to be significantly elevated ($p < 0.05$) at the FI site, registering 724.5 ± 216.7 µmol photons m^{-2} s^{-1}, in stark contrast to the DI site, which recorded 382.45 ± 288.86 µmol photons m^{-2} s^{-1}, and the RF site, where it was measured at 567.9 ± 230.7 µmol photons m^{-2} s^{-1}. The mean daily maximum VPD exhibited a higher value at the RF site (0.80 kPa ± 0.24), in comparison to the FI (0.73 kPa ± 0.25) and DI sites (0.59 kPa ± 0.16). Conversely, the mean daily VPD was observed to be lower at the DI site (0.29 kPa ± 0.09), when contrasted with FI (0.38 kPa ± 0.12) and RF (0.40 kPa ± 0.16) sites. The total precipitation recorded at the rainfed (RF) site amounted to 229 mm, characterized by an irregular temporal distribution that encompassed periods of successive dry days succeeded by intense rainfall episodes. Notably, towards the culmination of the crop cycle, a significant precipitation event was documented, with rainfall reaching 98 mm within a span of one week (101 to 107 DPP).The cumulative rainfall recorded for the full irrigation (FI) and deficit irrigation (DI) sites was higher, at 306 mm and 293 mm respectively, and exhibited a more uniform distribution. Nonetheless, a notably drier interval was observed at the FI site, spanning from 50 to 90 days. Water availability at the rainfed (RF) site was limited (soil water content, SWC, less than wilting point, WP) for approximately 71% of the total crop growth days. However, an increase in SWC was observed post-100 days, attributed to heightened rainfall. In contrast, at the deficit irrigation (DI) site, the SWC was closer to the WP than to the field capacity (FC) and fell below WP for approximately 40% of the time, predominantly during the early stages of crop growth (20–50 days post-planting, DPP) (Fig. 1).

3.2 Carbon fluxes of NEE, GPP, and R_{eco}

The cumulative GPP stood at 1087.56 ± 31 g C m^{-2} for full irrigation (FI), 838.69 ± 24 g C m^{-2} for deficit irrigation (DI), and 250.70 ± 7.8 g C m^{-2} for rainfed (RF) conditions. Meanwhile, cumulative ecosystem respiration (R_{eco}) sums were 775.6 ± 19 g C m^{-2} for FI, 821.39 ± 20 g C m^{-2} for DI, and 437.92 ± 11 g C m^{-2} for RF. Notably, at the FI site, differences between cumulative GPP and R_{eco} emerged early in the vegetative phase, with GPP consistently outpacing R_{eco} throughout the evaluation period, exhibiting a sigmoidal behavior pattern. At the DI site, cumulative GPP showed a

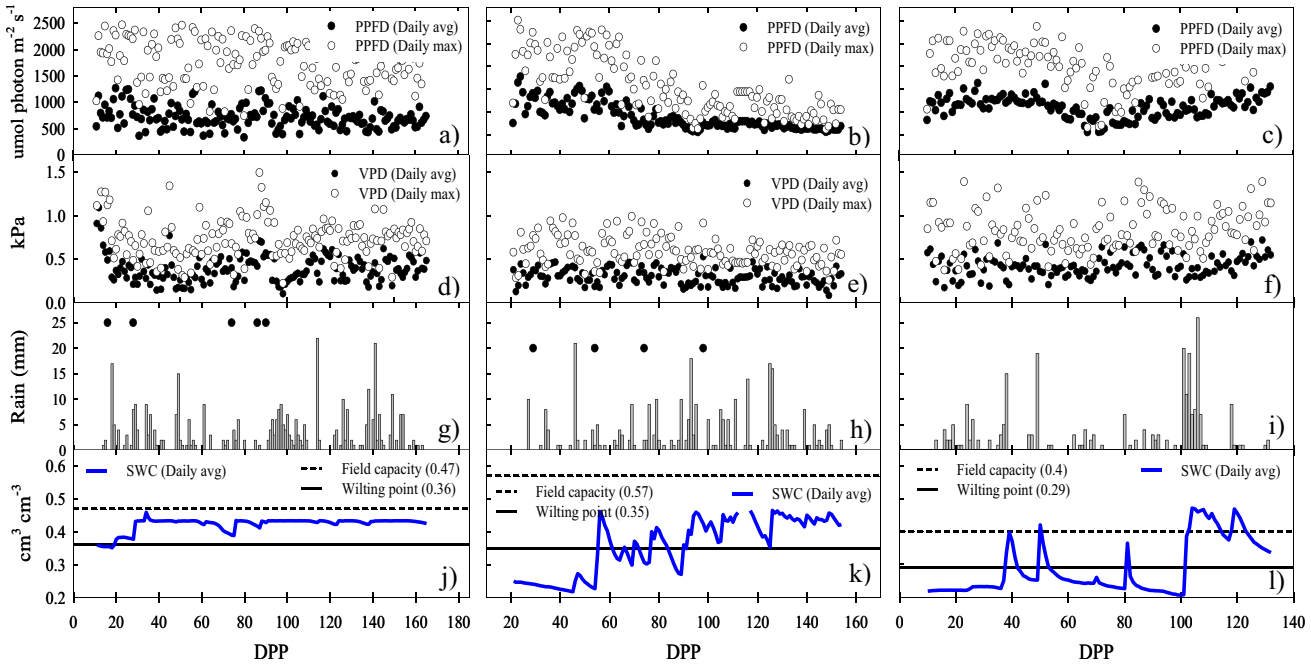

Fig. 1 Meteorological measurements for potato crop systems grown under different water management regimes [(a,d,g,j) full irrigation (FI); (b,e,h,k) deficit irrigation (DI); (c,f,i,l) rainfed conditions (RF)]. (**a**,**b**,**c**) photosynthetic active radiation, μmol photons m^{-2} s^{-1} (PPFD); (**d**,**e**,**f**) air vapor pressure deficit, kPa (VPD); (**g**,**h**,**i**) rainfall and irrigation times (black dots), mm; (**j**,**k**, **l**) soil water content, cm^3 $cm.^{-3}$ (SWC), measured at 0–20 cm depth is shown as daily mean values. Days post planting (DPP)

slight increase from 90 days post-planting (DPP) during the tuberization growth stage but dipped below R_{eco} levels during chemical haulm desiccation. At the RF site, R_{eco} surpassed GPP accumulation across all growth stages (Fig. 2). Initially, all sites exhibited positive accumulated NEE, but by the end of the vegetative stage, the FI site became a minor CO_2 sink (-26 ± 3.47 g C m^{-2}), while the DI and RF sites acted as CO_2 sources (16.91 ± 2.14 g C m^{-2} and 143 ± 5.65 g C m^{-2}, respectively). During tuberization and tuber bulking, both FI and DI sites acted as CO_2 sinks, with FI showing greater net carbon accumulation (-302 g C m^{-2}) compared to DI. Conversely, the RF site remained a CO_2 source throughout all growth stages (cumulative NEE of 175 ± 3.84 g C m^{-2} at the end of tuber bulking). Chemical haulm desiccation altered the trajectory of accumulated NEE, making it less negative, particularly at FI and DI sites from 140 and 135 DPP, respectively. Incorporating haulming emissions, cumulative NEE at the cycle's end for FI, DI, and RF was -311.96 ± 12.82, -17.3 ± 4.6, and 187.21 ± 3.84 g C m^{-2}, respectively (Fig. 2).

3.3 Crop development, carbon, and energy partitioning

At the FI site, the higher LAI (maximum LAI = 4.3 at 82 DPP) and SLA during the vegetative stage imply enhanced canopy expansion and the allocation of biomass towards thicker leaves. Conversely, at the DI and RF sites the pronounced decline in LAI (maximum LAI = 3.15 at 92 DPP and 3.14 at 78 DPP, respectively) and the rising trend of SLA during the vegetative growth at the RF site, and tuberization at the DI site, indicate a less expanded canopy with thinner leaves. On average 80 ± 14.6% of net radiation was partitioned to latent heat flux, with the peak energy allocation (LE/Rn = 85.3 ± 16.3%) coinciding with the tuberization stage, when the canopy reached its maximum LAI. During the tuber bulking stage, the observed decrease in the latent heat flux partitioning mirrored the trajectory of LAI during leaves senescence (Fig. 3a). At the DI site, the energy distribution for LE was slightly reduced (LE/Rn = 74 ± 8.89%) in comparison to the FI site. At peak LAI during tuberization, there was also a decrease in the partitioning of energy to latent heat flux from net radiation (LE/Rn = 76.6 ± 8%) (Fig. 3b). At the RF site, the Rn distribution for LE during the growth cycle averaged 52 ± 16.19%. Likewise, at maximum LAI, the LE allocation only reached 47.3 ± 15.8% (Fig. 3c). At the FI site, during the initial crop growth (0 – 30 DPP, low crop cover) GPP/R_{eco} ratio was < 1 meaning that R_{eco} was greater than GPP. Starting from 39 DPP, the GPP/R_{eco} ratio exceeded 1, with their values increasing in alignment with the LAI pattern, until surpassing 2 (between 2.6 and 2.8) during the peak LAI period in the tuberization stage. At the DI site, the GPP/R_{eco} ratio was initially below 1 (0–30 DPP). However, the increases observed during the tuberization and tuber bulking stages, ranging from 1 to 1.5,

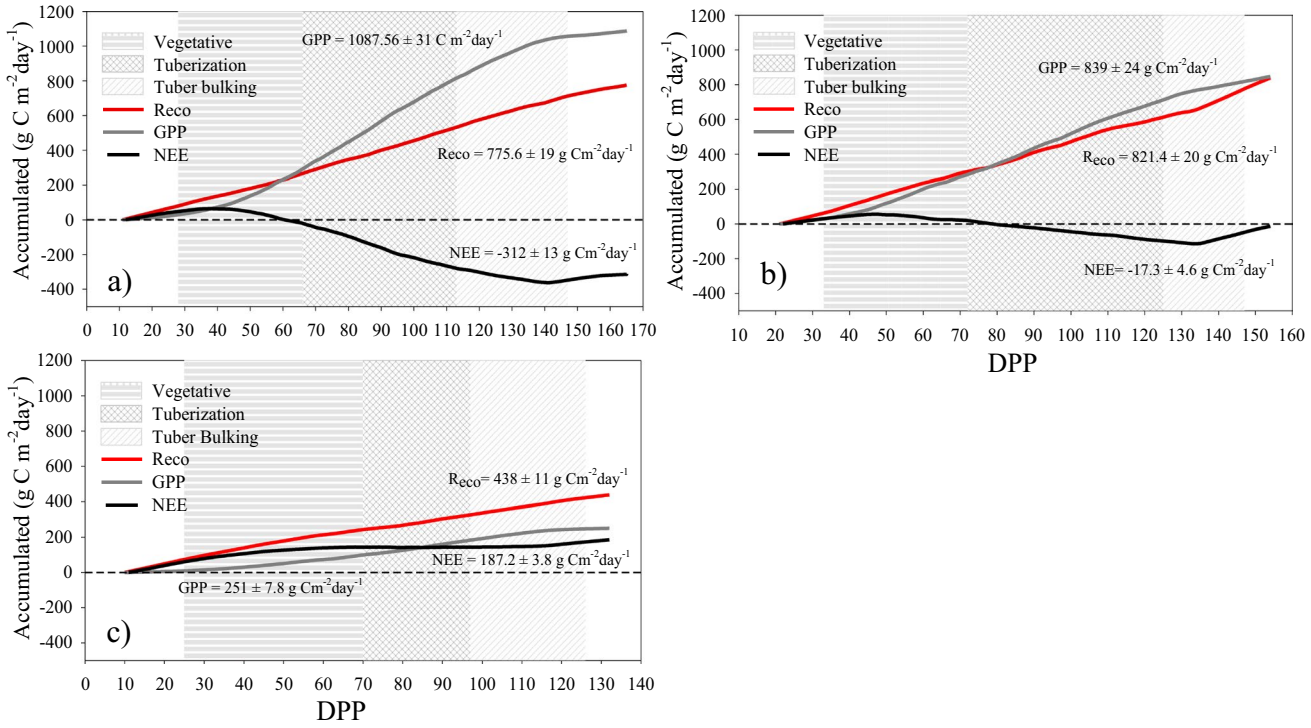

Fig. 2 Cumulative gross primary productivity (GPP), Ecosystem respiration (R_{eco}), and Net Carbon Ecosystem Exchange (NEE) during different potato growth stages (vegetative, tuberization, tuber bulking) in three different water regimes (**a**) full irrigation (FI), (**b**) deficit irrigation (DI), and (**c**) Rainfed (RF). Values inside figures correspond to NEE, GPP, and R_{eco} reached at the end of cycle (165 DPP, 152 DPP and 132 DPP for FI, DI and RF, respectively). Days post planting (DPP)

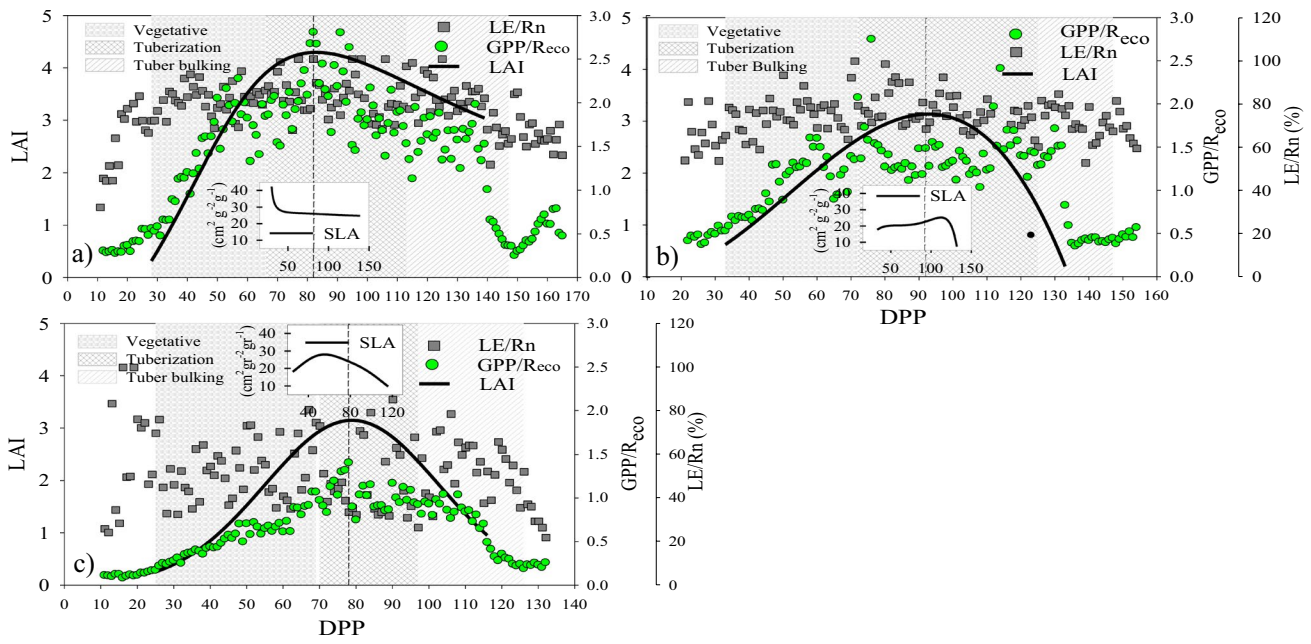

Fig. 3 Daily latent heat partitioning (LE/Rn), GPP/R_{eco} ratio, leaf area index (LAI) and specific leaf area (SLA), during different potato growth stages (vegetative, tuberization, tuber bulking) in three different water regimes (**a**) full irrigation (FI), (**b**) deficit irrigation (DI), and (**c**) Rainfed (RF) conditions. Dotted perpendicular line indicates maximum LAI. Days post planting (DPP)

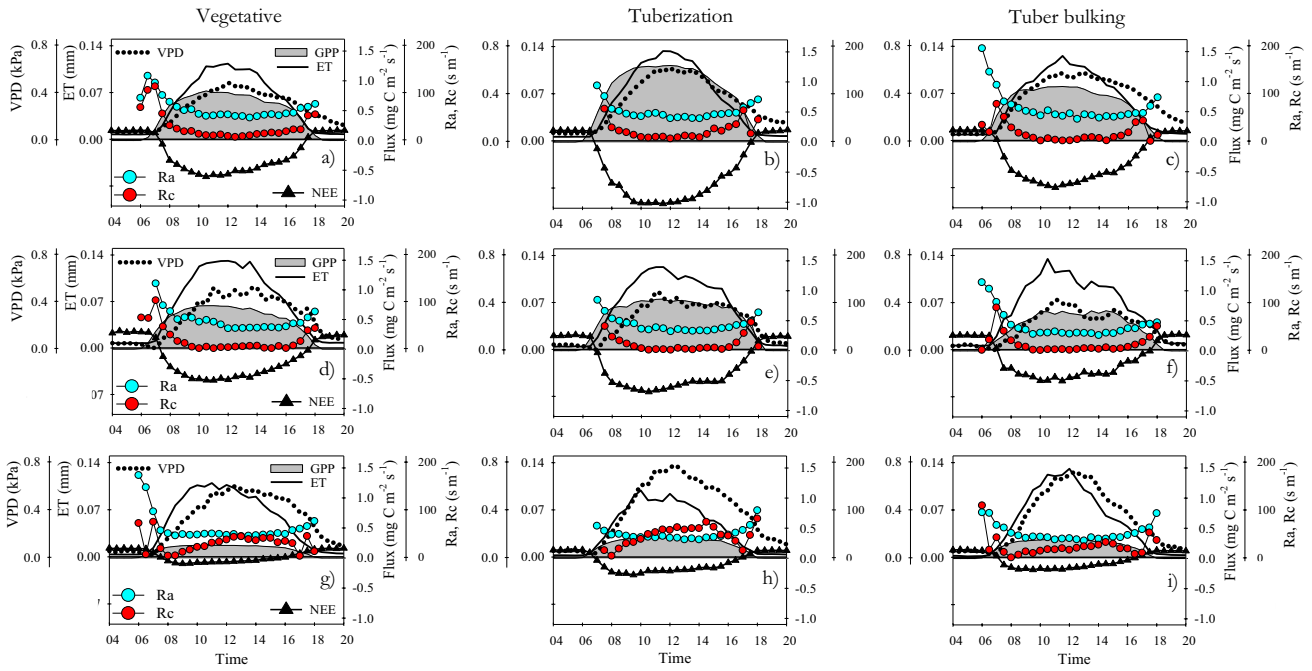

Fig. 4 Diurnal half-hourly evapotranspiration (ET), gross primary productivity (GPP), vapor pressure deficit (VPD), net carbon ecosystem exchange (NEE), aerodynamic resistance of the canopy (Ra) and the canopy stomatal resistance to vapor diffusion (Rc), during different potato growth stages (vegetative, tuberization, tuber bulking) in three different water regimes (**a**,**b**,**c**) full irrigation (FI), (**d**,**e**,**f**) deficit irrigation (DI), and (**g**,**h**,**i**) Rainfed (RF) conditions. The diurnal cycle begins at 04:00 h and ends at 20:00 h

were less pronounced compared to those at the DI site. At the RF site the GPP/R_{eco} ratio remained below 1 throughout almost the entire crop growth period.

3.4 Diurnal ET-GPP trends, synchrony and IWUE

The highest diurnal carbon and ET fluxes were observed at the FI site, especially during the tuberization stage (Fig. 4a-c). Half-hourly GPP showed an increasing trend throughout the day, peaking around 10:00—12:00 (0.83 mg m^{-2} s^{-1}, 1.27 mg m^{-2} s^{-1}, 0.77 mg m^{-2} s^{-1} for vegetative, tuberization, and tuber bulking stages, respectively). The ET had a similar pattern but peaked at midday reaching values of 0.11 mm, 0.13 mm, and 0.12 mm for vegetative, tuberization, and tuber bulking respectively. The highest sink activity was observed around 10:00 – 12:00, reaching NEE values of -0.6 mg m^{-2} s^{-1}, -1.025 mg m^{-2} s^{-1}, and -0.59 mg m^{-2} s^{-1} for vegetative, tuberization and tuber bulking respectively. At the DI site, the diurnal patterns of ET and GPP peaked earlier (around 09:00). GPP values decreased by 46.4% and 70.13% during the tuberization and tuber bulking stages, respectively (Fig. 4e, f). The sink activity (NEE) had also a reduction of 34% and 61% for tuberization and tuber bulking respectively, compared to the FI site. The RF site exhibited the lowest daytime carbon and ET fluxes. Peak ET values, attained at 09:00 during vegetative and tuberization stages were 11% and 31% lower, respectively, compared to analogous stages at the FI site (Fig. 4g, h). The sink activity was reduced by 85%, 73%, and 83% during vegetative, tuberization, and tuber bulking stages, respectively, compared to the same stages in the FI site. At FI and DI, a theoretically expected parabolic variation in the diurnal trend of Rc and Ra was observed across all growth stages (Rana et al. 1994; Alves et al. 1998; Perez et al. 2006; Irmak and Mutiibwa 2010; Monteith and Unsworth 2013; Lin et al. 2020). The Rc decreased from 30 m s^{-1} in the early morning (05:00 – 08:00), to less than 15 m s^{-1} from 10:00 to 15:00. Ra values were higher than Rc, with a range from 40 to 80 m s^{-1}, following a similar diurnal pattern across different growth stages. The VPD showed a progressive increase peaking around 11:00 – 12:00 reaching values of 0.5 kPa; 0.5 – 0.6 kPa, and 0.4 – 0.6 kPa, for vegetative, tuberization and tuber bulking stages, respectively. At the RF site, Rc showed an opposite pattern to the other sites. The linear increase from early morning to about 13:00—14:00 reached values of 45 m s^{-1}, 74 m s^{-1} and 32 m s^{-1} for vegetative, tuberization and tuber bulking stages, respectively. Ra was found to be similar to Rc, with values ranging from 30 to 60 m s^{-1} during the day. A diurnal increase in VPD was observed, with peak values of 0.6 kPa, 0.8 kPa, and 0.72 kPa for vegetative, tuberization, and tuber bulking stages, respectively, at 12:30 (Fig. 4).

Figure 5 shows a comparison between the daily cycles (normalized half-hourly intervals) from sunrise to sunset.

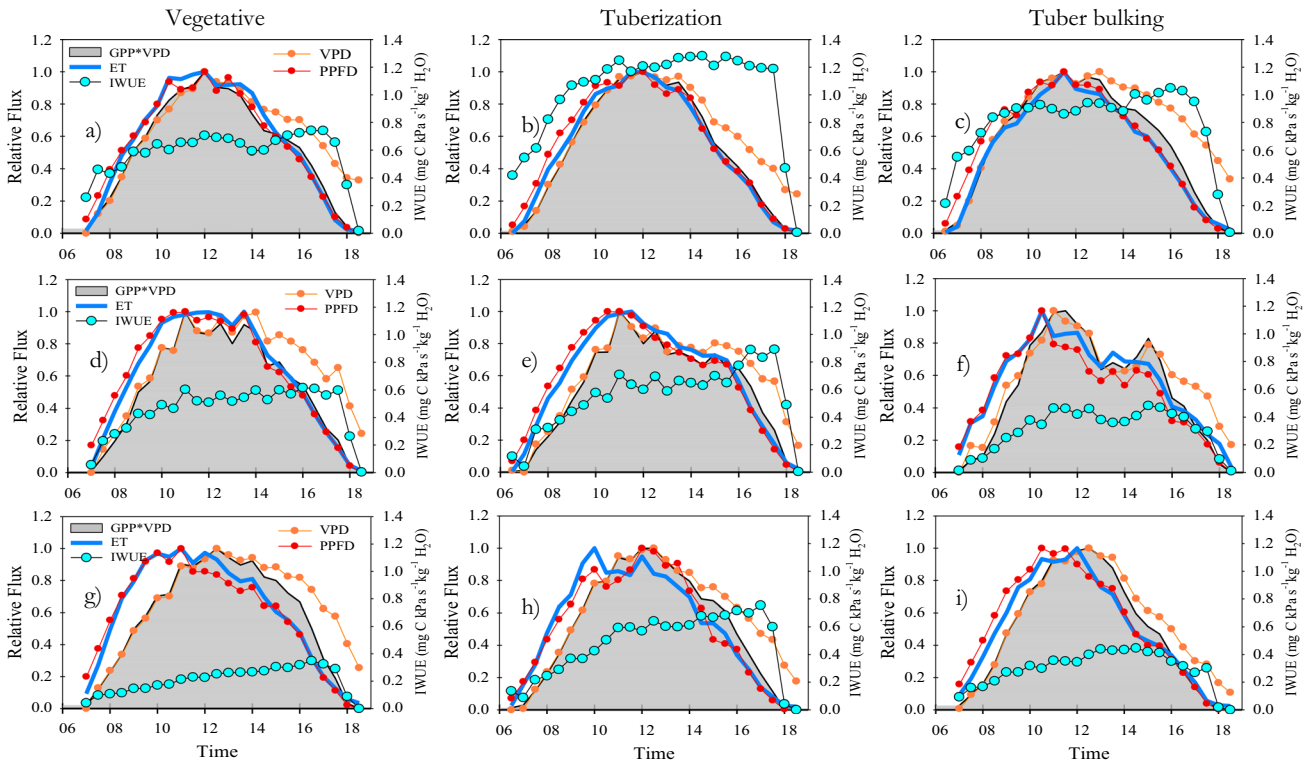

Fig. 5 Normalized diurnal variations in half-hourly PPFD, ET, GPP, VPD, GPP*VPD, IWUE during three different potato growth stages (vegetative, tuberization, tuber bulking) in three different water regimes (**a**,**b**,**c**) full irrigation (FI), (**d**,**e**,**f**) deficit irrigation (DI), and (**g**,**h**,**i**) Rainfed (RF) conditions. The diurnal cycle begins at 05:00 h and ends at 19:00 h

At the FI site, the relative fluxes of ET and GPP*VPD were proportional, coupled and synchronized, thus generating the highest IWUE values. Both ET and GPP*VPD peaked at the same time, around noon and closely track the relative changes of PPFD (Fig. 5a, b, c). At the DI site, the relative fluxes of ET and GPP*VPD are less proportional and synchronized, because the relative flux of GPP*VPD is smaller than ET in the morning. The peaks of both fluxes occurred simultaneously around 10:00 – 11:00 and dropped earlier in the day. The GPP*VPD signal loses synchrony with the normalized values of PPFD, and its variation is more coupled with changes in VPD. The normalized ET flux remains highly synchronized with PPFD during morning and afternoon (Fig. 5d, e, f). Under RF conditions, the relative fluxes of ET and GPP*VPD exhibited a lack of proportionality, showing decoupling, and poorly synchronization. The peaks of both fluxes did not align, as the relative flux of ET reached its maximum earlier than GPP. This time lags between these variables and the differences in the magnitude throughout the day, culminate in pronounced asynchrony and the lowest IWUE when compared to FI and DI sites. The relative flux of GPP was closely coupled with the VPD from morning until 14:00, while the relative ET flux was highly synchronized with PPFD. However, during the afternoon, notably in the vegetative growth and tuberization stages, discrepancies or diminished synchrony between ET and PPFD were observed, especially when compared to the FI and DI sites (Fig. 5g, h, i).

3.5 Environmental controls on NEE, GPP, ET, and IWUE-NEE relations

Logarithmic functions accurately characterized the scatter plot relationships between daily mean of half-hour GPP and GPP*DPV versus half-hour ET across all sites. The average GPP increases were 0.33, 0.21 and 0.06 mg C m^{-2} s^{-1} per unit of ET mm increase at FI, DI and RF sites, respectively. At the DI and RF sites, the increase of half-hourly GPP showed asymptotic values from 1 and 0.5 mg C m^{-2} s^{-1}, respectively, when half-hourly ET reached values around 0.1 mm and 0.05 mm respectively, indicating no increases of GPP beyond those ET values. At the FI site, the GPP – ET relation increased logarithmically without any clear threshold (Fig. 6a).

Over the whole crop growth, the individual half-hourly GPP*VPD and ET tend to be well correlated and well coupled ($r = 0.77$, $R^2 = 0.59$) at the FI site. GPP*VPD—ET coupling was slightly lower at the DI site ($r = 0.74$, $R^2 = 0.54$) and the lowest for the RF site ($r = 0.53$, $R^2 = 0.28$). Likewise, the instantaneous IWUE (the slopes of the linear

regressions) was greater for the FI site than DI and RF sites, being 4.7, 2.3 and 1.01 mg C kPa s^{-1} kg^{-1} H_2O, which indicates an improvement in water use under FI conditions (Fig. 6b).

The individual half-hourly NEE values were plotted against ET, PPFD, VPD and in Fig. 6c-e. Carbon sequestration activity exhibited an enhanced response and correlation to both ET and PPFD. The highest correlation was for NEE vs. ET, where the sink activity rate was -0.095 mg C m^{-2} s^{-1} $mm_{H2Ov}{}^{-1}$, -0.070 mg C m^{-2} s^{-1} $mm_{H2Ov}{}^{-1}$ and -0.020 mg C m^{-2} s^{-1} $mm_{H2Ov}{}^{-1}$ at FI, DI and RF sites, respectively (Fig. 6c). Regarding NEE vs PPFD, at the FI site the carbon sink activity increased progressively (NEE decreases) until approximately 1500 mmol photons m^{-2} s^{-1} at average rate of -0.06 mg C m^{-2} s^{-1} per PPFD mmol photons m^{-2} s^{-1}. At the DI site, NEE had a lower response to PPFD; the sink activity increased until 750 mmol photons m^{-2} s^{-1} at a rate of -0.04 mg C m^{-2} s^{-2} per PPFD mmol photons m^{-2} s^{-1}. Under RF conditions no evidence of changes in carbon sink activity beyond 300 mmol photons m^{-2} s^{-1} was observed. The sink activity rate was -0.01 mg C m^{-2} s^{-2} per PPFD mmol photons m^{-2} s^{-1} (Fig. 6d).

Although the correlation between individual half-hourly net ecosystem exchange (NEE) values and vapor pressure deficit (VPD) was low, an increase in carbon sink activity was noted with rising VPD up to 0.6 kPa at the FI and DI sites. At the RF site, the NEE decreased around a VPD = 0.3 kPa, and a reduction in sink capacity and positive NEE values were observed as VPD increased (Fig. 6e). The response of NEE to IWUE differed cross sites (Fig. 6f). At the FI site, the average carbon sink activity increased with IWUE until IWUE = 6 mg C kPa s^{-1} kg^{-1} H_2O. At the DI and RF sites, the peak carbon sequestration activity was observed near IWUE values of approximately 2 mg C KPa s^{-1} kg^{-1} H_2O, and IWUE ~ 1 mg C kPa s^{-1} kg^{-1} H_2O, respectively. Beyond these IWUE thresholds, a significant reduction in the carbon sequestration activity was observed (Fig. 6).

3.6 ET-GPP coupling and omega

At the FI site, the daily GPP*VPD vs ET correlation coefficient (r) exceeded 0.85 during 78% of crop cycle (154 days) and ranged from 0.75 to 0.84 during 14% of cycle. During almost all vegetative stage, daily r coefficient was between 0.66—0.84, indicating an ET-GPP decoupling. From vegetative growth stage, IWUE progressively increased to maximum values of 22 and 17 mg C kPa day^{-1} kg^{-1} H_2O during the tuberization and tuber bulking stages, respectively. At the DI site, 52% of crop cycle (147 days) had correlation coefficients above 0.85. An ET-GPP decoupling (r coefficient between 0.55—0.84) was observed during tuberization (in about 48% of stage) and tuber bulking (74% of stage). IWUE was lower compared to the FI site, reaching maximum values of 14 and 6.5 mg C kPa day^{-1} kg^{-1} H_2O during tuberization and tuber bulking respectively (Fig. 7). The largest variability in the correlation coefficient was observed at the RF site. Only 41% of crop cycle (130 days) had a r coefficient greater than 0.85. During vegetative and tuberization stages, the daily r coefficient varied from 0.3 to 0.84, and 0.48 to 0.84, respectively. The RF site exhibited the lowest IWUE values primarily during vegetative growth (IWUE < 5 mg C kPa day^{-1} kg^{-1} H_2O) and tuberization (max IWUE = 12 mg C kPa day^{-1} kg^{-1} H_2O). The omega values close to 1 ($\Omega \sim 0.8$—0.9), indicate that at both the FI site and the DI site, the net radiation is the main contributor to the evapotranspiration process. Therefore, vegetation is completely decoupled from the atmospheric conditions. At the RF site, lower omega values ($\Omega \sim 0.6$) were observed mainly in the vegetative and tuber bulking stages, indicating an increase in coupling, and a greater control of ET by vegetation in terms of surface conductance and VPD (Fig. 7).

4 Discussion

4.1 Crop development, surface resistance and carbon—water fluxes

The highest water and carbon fluxes were observed under the well-watered conditions at the FI site. Over 80% of the net radiation was allocated to LE, indicating that the predominant consumption of energy was for evapotranspiration processes. The largest GPP/R_{eco} ratio, mainly during the tuberization stage ($GPP/R_{eco} > 2$), implies that autotrophic respiration widely dominates the carbon fluxes, reflecting elevated rates of photosynthesis (GPP), and CO_2 sequestration (Falge et al. 2001, 2002; Cabral et al. 2013; Rana et al. 2016). As a result, the potato crop at the FI site was a larger CO_2 sink when compared to the other sites. These results suggest that higher LAI and SLA influenced the energy partitioning and carbon fluxes (Haiqiang et al. 2010; Jia et al. 2014; Kang et al. 2015; Shao et al. 2015; Van Dijke et al. 2020). It was observed that the increase in energy consumption to LE and autotrophic activity (respiration and photosynthesis) were directly associated with increases in LAI and SLA. The decline behavior of the SLA during the initial canopy growth implies a leaf thickening (increases in length and palisade cell layers). This phenomenon leads to higher transpiration efficiency, photosynthetic rates, and an overall increase in plant carbon demand (Wright et al. 1994; Evans and Poorter 2001; Jullien et al. 2009; Goorman et al. 2011; Vadez et al. 2014; Weraduwage et al. 2015; Gonzalez-Paleo and Ravetta 2018). LAI has been reported as the main determinant of daily GPP, and ET variations (Jongen et al. 2011; Souza et al. 2012; Gondim et al. 2015; Van Dijke et al. 2020; Martínez-Maldonado et al. 2021). The magnitude of water

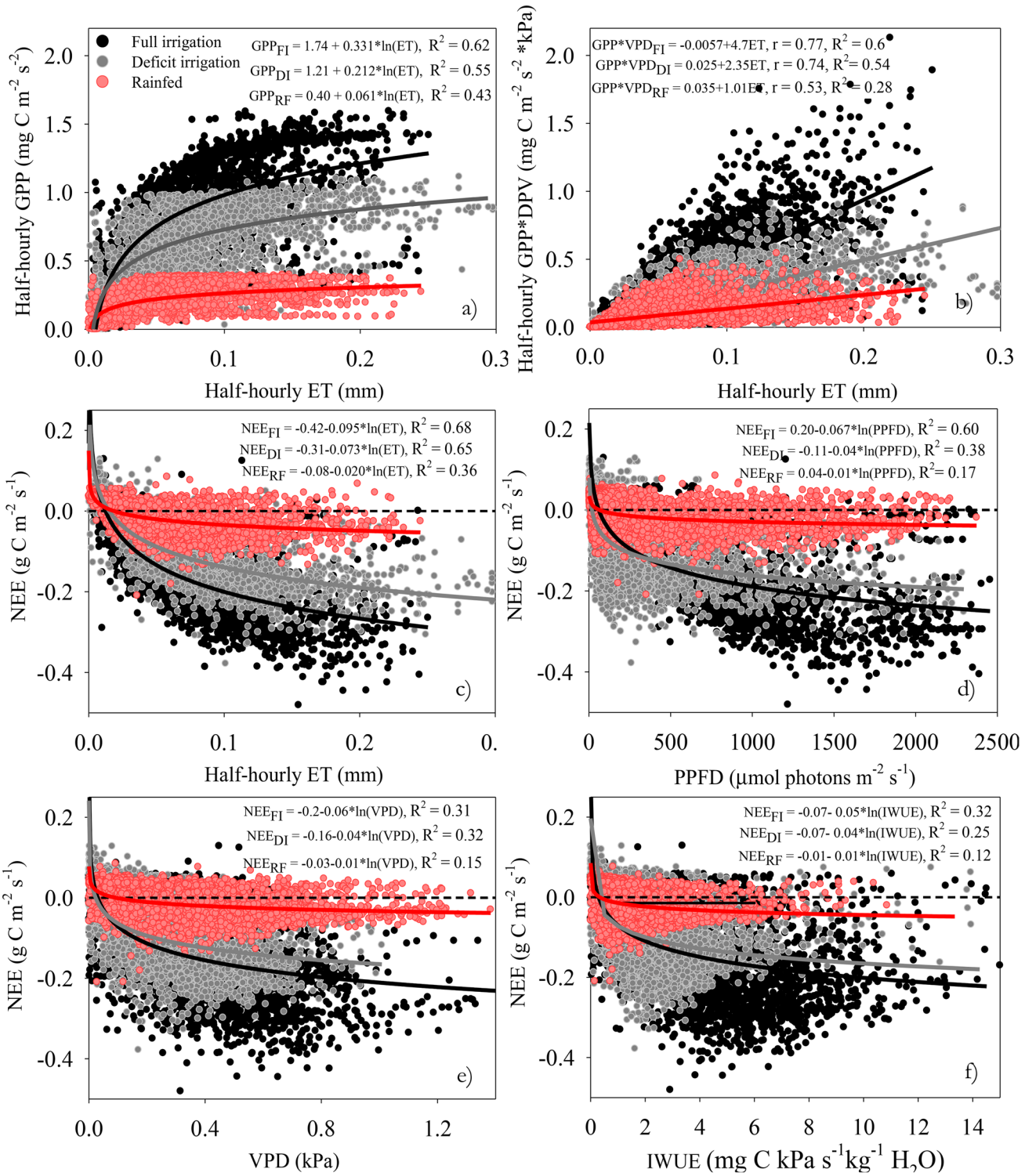

Fig. 6 Overall half-hourly relationship between (**a**) GPP and ET; (**b**) GPP*VPD and ET; (**c**) NEE and ET; (**d**) NEE and PPFD; (**e**) NEE and VPD; and (**f**) NEE and IWUE in three potato water regimes cropping systems [full irrigation (FI) deficit irrigation (DI) rainfed conditions (RF)]. Also shown is the correlation coefficient, determination coefficient, linear GPP*VPD and ET, and logarithmic functions. The p values of all regressions are < 0.1

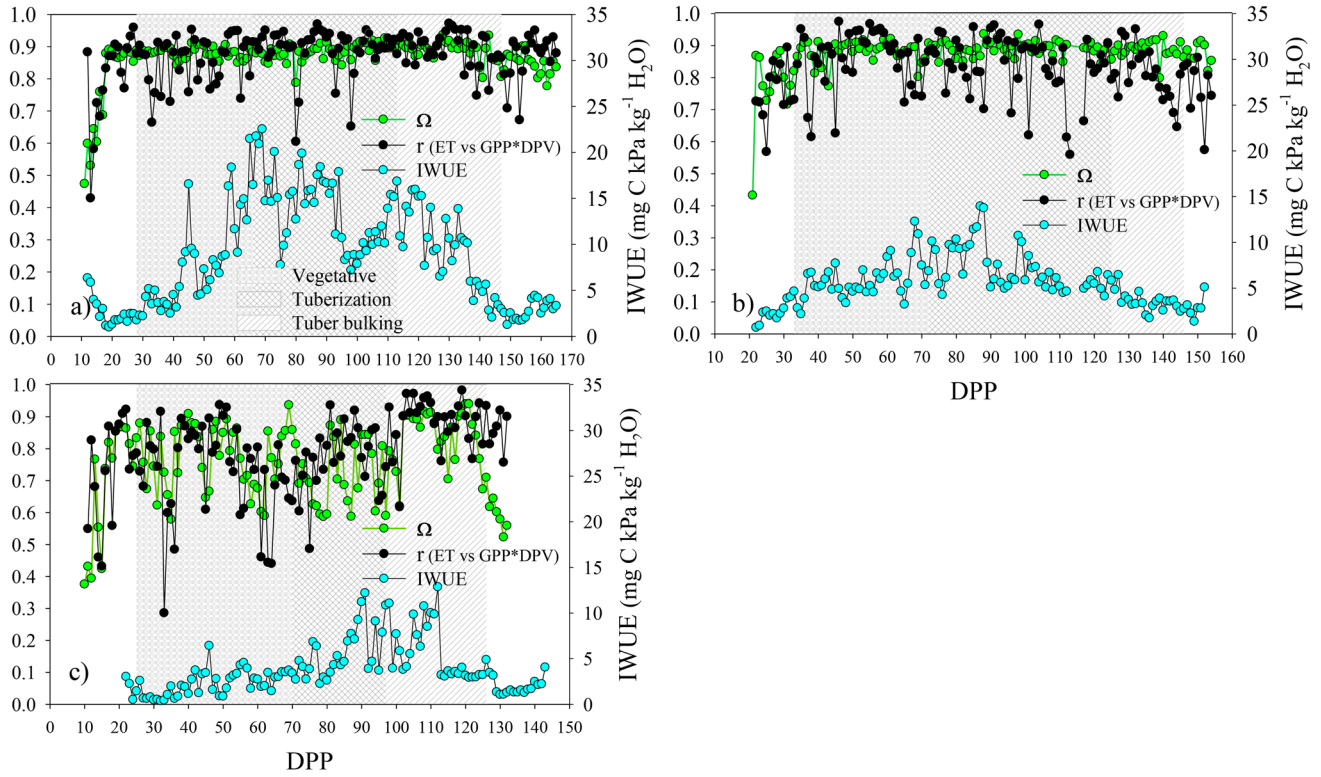

Fig. 7 Daily correlation coefficients (r) between GPP*VPD and E, omega coefficient, and IWUE during different potato growth stages (vegetative, tuberization, tuber bulking) in three different water regimes (**a**) full irrigation (FI), (**b**) deficit irrigation (DI), and (**c**) Rainfed (RF) conditions. Days post planting (DPP)

and carbon fluxes partially depends on canopy magnitude and LAI works as an indicator of the total amount of foliage for transpiration, light interception, and carbon assimilation (Van Dijke et al. 2020).

At the DI site, there was a slight decrease in the energy partitioning to latent heat, however, autotrophic and CO_2 sink activities were lower than in the FI site as occurs in drought-stressed ecosystems (Falge et al. 2002). The water deficit during early crop growth caused reductions in canopy growth (LAI and SLA), which through less total leaf mass for photosynthesis, less thick leaves, and fewer carbon requirements for mass increase (showed as an ascending behavior of SLA) directly affected the magnitude of carbon fluxes (GPP and R_{eco}) (Fatichi et al. 2014; Nadal-Sala et al. 2021). At the RF site, only 50% of energy was allocated to LE, and the crop acted as a net CO_2 source because of the water deficit during 70% of crop growth. Carbon fluxes were dominated by soil heterotrophic activity, and less carbon was used for crop growth due to the very low autotrophic activity (Falge et al. 2001, 2002; Cabral et al. 2013; Rana et al. 2016). Water deficit caused the highest reductions in LAI, and SLA, resulting in a poorly expanded canopy with thin leaves (Wright et al. 1994; Jullien et al. 2009; Weraduwage et al. 2015; Gonzalez-Paleo and Ravetta 2018) and highly reduced carbon requirements for crop growth.

In well-watered conditions (FI) (at the diurnal half-hourly scale), elevated ET, GPP, and sink activity (more negative NEE) were observed during the lowest Rc, which evidence an intense carbon–water exchange under a low bulk resistance to mass transfer (Amer and Hatfield 2004; Aires et al. 2008; Kumagai et al. 2008; Souza et al. 2012; Wehr and Saleska 2021) which supports a higher CO_2 sequestration activity. Midday Rc values around 15 s m^{-1} were similar to those reported for potato by Amer and Hatfield (2004) and (López-Olivari et al. 2022) and lower than those reported by (Kjelgaard and Stockle 2001) (40 s m^{-1}).

At the DI site, ET continued at a high rate while there was a high restriction in the GPP and NEE fluxes. The diurnal Ra > Rc and high ET evidenced that the canopy was not capable of reducing water losses during the water deficit events (Fereres and Soriano 2007; Spinelli et al. 2018). The low Rc suggests that GPP and NEE fluxes were likely constrained by ecosystem-scale non-stomatal limitations of photosynthesis (NSL) (Jarvis 1985; Reichstein et al. 2002; Migliavacca et al. 2009) via a less developed canopy with lower autotrophic activity (Fatichi et al. 2014; Nadal-Sala et al. 2021) and a lower radiation, declining the

photosynthetic performance (Xu and Baldocchi 2004; Obidiegwu et al. 2015; Nelson et al. 2018; Yang et al. 2019; De La Motte et al. 2020; Nadal-Sala et al. 2021). Under rainfed conditions (RF), diurnal canopy resistance was increased in response to VPD increases (up to 5 times larger than at the FI site when VPD ≈ 0.8 kPa) (Aires et al. 2008; Silva et al. 2017; Sutherlin et al. 2019; Alves et al. 2022) resulting in a high restriction of diurnal ET and GPP across all growth stages. Under this severe water deficit, VPD exerted negative physiological feedback on LE (Teixeira et al. 2008) since energy partitioning depends on surface resistance (Li et al. 2005; Chen et al. 2009; Kang et al. 2015). The lower LE/Rn observed at this site is a result of a higher water vapor gradient (higher VPD), which raised Rc by closing the stomata (Spinelli et al. 2018). Diurnal GPP was more restricted than ET as has been reported under drought conditions (Spinelli et al. 2016, 2018; Nelson et al. 2018; Yang et al. 2019; De La Motte et al. 2020). While ET is only limited by the available energy and/or Rc to water vapor transfer, GPP is limited by the joint effect of canopy resistance, mesophyll conductance, the rate at which chloroplasts fix carbon (Steduto and Hsiao 1998; Spinelli et al. 2016, 2018), and the additional non-stomatal limitations of photosynthesis (NSL).

4.2 ET-GPP coupling, NEE-IWUE relations and environmental controls

At the FI site, the diurnal normalized cycles of ET and GPP*DVP were proportional and largely synchronized (Beer et al. 2009; Nelson et al. 2018; Aguilos et al. 2021), indicating that the amount of carbon entering the canopy is proportional to the water leaving it (Mallick et al. 2016; Nelson et al. 2018; Gentine et al. 2019; Van Dijke et al. 2020). The synchrony and proportionality of water and carbon fluxes are also reflected in the higher response of GPP to ET, as well as in the high correlation between overall half-hour GPP*VPD and ET (Loader et al. 2011; Leonardi et al. 2012; Battipaglia et al. 2013; Grossiord et al. 2014; Zhou et al. 2014) where carbon assimilation was sustained even at the utmost water vapor flux (Katul et al. 2010), resulting in a greater IWUE and more negative NEE values. The higher correlation between PPFD and water and carbon fluxes reveals that light was the main driver for diurnal GPP and ET (Eamus et al. 2016; Liu et al. 2021). Water and carbon exchange remained coupled as more PPFD was intercepted by the canopy (Wilson et al. 2001; Arkebauer et al. 2009; Samanta et al. 2020), which supported the increase of carbon sequestration (NEE gets more negative) as PPFD increased even at values beyond 1500 mmol photons m^{-2} s^{-1}. As a result, PPFD was also the primary driver controlling daytime NEE (explaining 60% of the variations in overall half-hourly NEE). These results confirm the hypothesis that, under well-irrigated conditions, the tight coupling between GPP and ET fluxes driven mainly by PPFD, generates a higher IWUE and, consequently, a greater sink activity.

At the DI site, ET and GPP*DVP normalized cycles became uncoupled, losing synchronization and proportionality. The maximum peaks reached earlier indicate that the time for intense transpiration activity and water-carbon exchange was restricted (almost 2 h), which constrains IWUE. In this lower ET – GPP*DPV coupling, ET remains high, but intra-leaf factors and other non-stomatal limitations to photosynthesis are slowing carbon fixation, constraining GPP and changing the IWUE by non-VPD effects (Beer et al. 2009; Nelson et al. 2018). At the RF site, the great restrictions in ET and GPP under severe water deficit caused high asynchrony, ET-GPP*DPV decoupling, and the lowest IWUE (Reichstein et al. 2002; Migliavacca et al. 2009). In our analysis, carbon–water decoupling results from an unbalanced constraint for ET and GPP fluxes (affecting GPP > ET) imposed by VPD. It seems that increases in Rc in response to higher VPD primarily affect the GPP since the diurnal normalized ET remains in high sync and correlation to PPFD, but diurnal GPP was more synchronized and correlated with VPD causing a time lag between their maximum peaks. Further, under severe and prolonged water deficit, additional restrictions to GPP arise from non-stomatal photosynthesis limitations (NSL), which include reduced mesophyll conductance (Flexas et al. 2012; De La Motte et al. 2020; Evans 2021), photochemical and enzymatic limitations like the destruction of chlorophyll components, disorganization of chloroplast ultrastructure, enzyme inactivation and photo-inhibition (Flexas and Medrano 2002; Flexas et al. 2004; Niinemets et al. 2006; Galmés et al. 2007; Varone et al. 2012; Sugiura et al. 2020).

At both DI and RF sites, the scarce response of GPP to ET as well as the low correlation between overall half-hour GPP*VPD and ET indicated an overall decoupling between carbon and water fluxes and limitations for inherent water use efficiency. After GPP values of 0.5 mg C m^{-2} s^{-2}, increases in ET no longer brought additional increases in GPP. This water loss with no productive purposes means that the crop cannot restrict water losses or maximize its carbon gains under water-limiting conditions. The resulting lowest sink activity observed at DI and RF sites is in part attributed to lower coupling between ET and GPP fluxes, represented in a lower IWUE. However, the relationship proposed in the IWUE would only explain the variability of the negative values of the NEE, since they are associated with the activity of the GPP. From our point of view, the lower number of negative NEE values and the persistent positive values are consequence of both the low IWUE and the greater role of R_{eco} in the carbon balance. Under water deficit, the increase in the R_{eco} flux is either by lower autotrophic activity from plants or increased heterotrophic activity from the soil (Falge et al. 2002; Cabral et al. 2013; Rana et al. 2016). At the DI

site, the response of sink activity (NEE) to ET was high, despite the water deficit water vapor flux was a main driver of carbon sequestration. The NEE had a lower response to PPFD (NEE decreased linearly around 750 mmol photons m^{-2} s^{-1}), indicating that the lower values of PPFD could be a limiting factor for sink activity. At the RF site, sink activity stalls or saturates at low ET, PPFD, and VPD. The low response to these environmental determinants could be due to both the lower GPP and the fact that the carbon balance is mainly dominated by the high respiration of the ecosystem, as a consequence of physiological and biophysical changes previously discussed.

4.3 ET-GPP coupling and the omega role

Quantification of the coupling or decoupling magnitude between water and carbon fluxes by daily correlation coefficient (r) of GPP*VPD vs ET, reveals that most of the growth days at the FI site exhibited a high daily correlation coefficient for ($R > 0.85$), signifying a tight coupling and synchronization between carbon and water fluxes. This observation aligns with prior findings, which have also documented high correlations between these two fluxes on days characterized by ample water availability (Beer et al. 2009; Nelson et al. 2018). The daily omega values oscillated between ~ 0.8 to 0.9, a range consistently documented in the literature for horticultural crops experiencing no stress (Jarvis and Mcnaughton 1986; McNaughton and Jarvis 1991; Ferreira 2017). These values are marginally elevated compared to $\Omega = 0.7$, as reported by Brown (1976) for potato. This Ω near to 1 implies a condition based on Ra > Rc as previously identified at the FI site. The elevated Ra observed between leaf surfaces and the air above the canopy indicates reduced diffusivity of water vapor from the leaves, thereby making ET more significantly controlled by incoming radiation and less influenced by stomatal conductance and canopy resistance (Jarvis 1985; Jarvis and Mcnaughton 1986; McNaughton and Jarvis 1991; Steduto and Hsiao 1998; Zhang et al. 2016; Sutherlin et al. 2019). The omega $\Omega \rightarrow 1$ gives a substantial advantage to the potato canopy, since transpiration remains unaffected by stomatal conductance and soil water fluctuations (Sutherlin et al. 2019; Martinez Maldonado and Marin 2023). The tightly coupled carbon and water fluxes, combined with the absence of canopy resistance constraints, enhanced the potato ecosystem's efficiency in optimizing carbon gains relative to water losses as crop growth advanced (Katul et al. 2010). This phenomenon is reflected in the daily patterns of IWUE, which are significantly influenced by the Leaf Area Index (LAI) and growth stages of the crop (Beer et al. 2009). Such an improvement in IWUE implies elevated plant transpiration efficiency, and a favorable effect on the plant's carbon balance (increased sink activity) (Leonardi et al. 2012) as previously discussed for the FI site.

At the DI site, a carbon–water decoupling ($r < 0.84$) was noted during tuberization and tuber bulking phases, accompanied by the greatest reductions in IWUE compared to the FI site. The daily omega coefficient, ranging from ~ 0.8 to 0.9, indicates that ET was predominantly controlled by the Ra and incoming radiation rather than by canopy resistance and VPD (Jarvis 1985; Jarvis and Mcnaughton 1986). This suggests that there were no limitations in ET, nor was there increased canopy control over the fluxes. The evidence presented in this study suggest that non-stomatal limitations on the GPP related to reduced canopy growth, thinner leaves, a decline in autotrophic respiration, and diminished response to PPFD constitute de underlying causes of decoupling and diminished IWUE. It is important to highlight that there are no stomatal/surface resistance limitations based on the high omega values, which indicate no significant alterations in Rc and Ra in comparison to the FI site.

At the RF site, for most of the crop growth period (over 80%), the ET and GPP fluxes exhibited uncoupling and desynchronization ($r < 0.84$), predominantly during vegetative growth and tuberization phases; Markedly low values of the correlation coefficient were observed (r ~ 0.4), revealing significant discrepancies between diurnal trends of carbon and water fluxes. Consequently, the RF site experienced the most pronounced reductions in daily IWUE throughout the entire crop growth period. The Omega coefficient (Ω) was generally lower compared to FI and DI sites, with the lowest values (omega ~ 0.6) predominantly observed during the vegetative and tuber bulking stages. These reduced Ω values suggest that ET and GPP were primarily controlled by VPD and Rc (Jarvis and Mcnaughton 1986; Aires et al. 2008; Nassif et al. 2014; Martinez Maldonado and Marin 2023) under rainfed conditions prevalent at the RF site. Both omega and the correlation coefficient (r) exhibited analogous trends of variation throughout the crop growth cycle. This observation suggests that on days when omega and r decrease concurrently, there is a pronounced ET-GPP decoupling due to an increased degree of canopy control over this fluxes in response to elevated VPD, which significantly impacts IWUE. However, as previously discussed, this elevated Rc may impose a greater restriction on photosynthesis (GPP) than on ET (Jarvis 1985; Steduto and Hsiao 1998; Spinelli et al. 2016, 2018) and unbalance constraint occurs over GPP due to both stomatal and non-stomatal limitations affecting photosynthesis. Other researchers have reported a declining trend in omega under water deficit conditions, attributed to an increase in canopy resistance and a decrease in aerodynamic resistance (Spinelli et al. 2016; De Kauwe et al. 2017; Ferreira 2017; Silva et al. 2017; Sutherlin et al. 2019) which agrees with the results presented in this study.

5 Conclusions

In irrigated potato systems there is a greater sink activity (negative NEE), attributed to higher GPP and ET fluxes, as well as to the high intrinsic water use efficiency. The higher photosynthetic CO_2 gain per unit of evapotranspired water is linked to a high proportionality and synchrony of water and carbon diurnal fluxes, both mainly controlled by the radiative environment. The canopy exerts significant influence on both GPP and ET fluxes, primarily attributable to the larger base area for mass exchange (high LAI and thick leaves), high autotrophic activity, low canopy stomatal resistance (Rc), and a decoupled condition from the atmosphere ($\Omega \sim 1$). This could imply that expanding potato irrigation areas could enhance carbon sequestration in potato fields through improved water use efficiency, yields, and productivity. Irrigation could be an important mitigation practice within sustainable productive intensification schemes.

Under water deficit conditions of the rainfed system, the lower sink capacity and carbon source activity (less negative or positive NEE) is due to limitations in GPP and ET fluxes and a lower IWUE implying a lower coupling and synchrony between water and carbon diurnal fluxes. The high atmospheric evaporative demand (high VPD) and very low SWC cause a smaller canopy (low LAI and thin leaves) with increases in canopy stomatal resistance (Rc) because of rises in canopy coupling to the atmosphere ($\Omega \sim 0$). These results indicate that in potato crop the mechanism control to minimize excessive water loss (lowering ET by increasing canopy coupling to the atmosphere) works only at severe water deficit. Under moderate water deficit ET remains at high rates because it is still dependent on available radiation and to a lesser extent the surface resistance.

Through the analysis of both metrics, omega, and correlation coefficients, we distinguished the possible causes of lower IWUE and the influence of environmental VPD and PPFD controls of ET and GPP fluxes. These metrics and their underlying theory could give new information about carbon–water interactions and it can be used as a tool to further understand the impact of drought on potato sink activity.

Acknowledgements This work is part of a larger project in Corporación Colombiana de Investigación Agropecuaria (AGROSAVIA) named Sistema de Información Agroclimática del cultivo de la papa en la región de Cundinamarca, Colombia (SIAP). We thank Zahara Lucia Lasso Paredes, Jose Alfredo Molina Varón, and Óscar Dubán Ocampo Páez, for their contribution in the equipment installation process, and farmers Santiago Forero and Alejandro Forero for providing a suitable lot for the study.

Author contributions F.E.M.M: Conceptualization, Methodology, Formal analysis, Investigation, Writing original draft, Writing review & editing. A.M.C.M: Methodology, Investigation, Funding acquisition, Project administration, Supervision, Writing review & editing. G.A.G.V: Software, Data curation, Methodology, Investigation, Writing review & editing. F.R.M.: Conceptualization, Supervision, Writing review & editing. All authors read and approved the final manuscript. All authors contributed to the study conception, design and reviewed the manuscript.

Funding Open Access funding provided by Colombia Consortium. This research was funded by the Fondo de Ciencia, Tecnología e Innovación del Sistema General de Regalías, administered by the Fondo Nacional de Financiación para Ciencia, Tecnología e Innovación—Francisco José de Caldas, Programa Colombia BIO, Gobernación de Cundinamarca and Ministerio de Ciencia, Tecnología e Innovación (MINCIENCIAS), and Corporación Colombiana de Investigación Agropecuaria (AGROSAVIA). Research work is part of a larger project in Corporación Colombiana de Investigación Agropecuaria (AGROSAVIA) named Sistema de Información Agroclimática del cultivo de la papa en la región de Cundinamarca, Colombia (SIAP).

Data availability The datasets generated during and/or analysed during the current study are not publicly available due to they are protected under the copyright of AGROSAVIA but are available on reasonable request.

Declarations

Competing interests The authors declare no competing interests.

References

Abbate PE, Dardanelli JL, Cantarero MG et al (2004) Climatic and water availability effects on water-use efficiency in wheat. Crop Sci 483:474–483. https://doi.org/10.2135/cropsci2004.0474

Aguilos M, Sun G, Noormets A, et al (2021) Ecosystem productivity and evapotranspiration are tightly coupled in loblolly pine (Pinus taeda l.) plantations along the coastal plain of the southeastern U.S. Forests 12:18. https://doi.org/10.3390/f12081123

Aires LM, Pio CA, Pereira JS (2008) The effect of drought on energy and water vapour exchange above a mediterranean C3/C4 grassland in Southern Portugal. Agric for Meteorol 148:565–579. https://doi.org/10.1016/j.agrformet.2007.11.001

Ali S, Xu Y, Ma X et al (2017) Planting patterns and deficit irrigation strategies to improve wheat production and water use efficiency under simulated rainfall conditions. Front Plant Sci 8. https://doi.org/10.3389/fpls.2017.01408

Alves I, Perrier A, Pereira LS (1998) Aerodynamic and surface resistances of complete cover crops: how good is the "big leaf"? Trans Am Soc Agric Eng 41:345–351. https://doi.org/10.13031/2013.17184

Alves JDN, Ribeiro A, Rody YP, Loos RA (2022) Energy balance and surface decoupling factor of a pasture in the Brazilian Cerrado. Agric For Meteorol 319. https://doi.org/10.1016/j.agrformet.2022.108912

Amer KH, Hatfield JL (2004) Canopy resistance as affected by soil and meteorological factors in potato. Agron J 96:978–985. https://doi.org/10.2134/agronj2004.0978

Arkebauer TJ, Walter-Shea EA, Mesarch MA et al (2009) Scaling up of CO_2 fluxes from leaf to canopy in maize-based agroecosystems. Agric for Meteorol 149:2110–2119. https://doi.org/10.1016/j.agrformet.2009.04.013

Aubinet M, Moureaux C, Bodson B et al (2009) Carbon sequestration by a crop over a 4-year sugar beet/winter wheat/seed potato/winter wheat rotation cycle. Agric for Meteorol 149:407–418. https://doi.org/10.1016/j.agrformet.2008.09.003

Battipaglia G, Saurer M, Cherubini P et al (2013) Elevated CO_2 increases tree-level intrinsic water use efficiency: Insights from carbon and oxygen isotope analyses in tree rings across three forest FACE sites. New Phytol 197:544–554. https://doi.org/10.1111/nph.12044

Beer C, Ciais P, Reichstein M et al (2009) Temporal and among-site variability of inherent water use efficiency at the ecosystem level. Global Biogeochem Cycles 23:1–13. https://doi.org/10.1029/2008GB003233

Bierhuizen JF, Slatyer RO (1965) Effect of atmospheric concentration of water vapour and CO_2 in determining transpiration-photosynthesis relationships of cotton leaves. Agric Meteorol 2:259–270. https://doi.org/10.1016/0002-1571(65)90012-9

Birch PRJ, Bryan G, Fenton B et al (2012) Crops that feed the world 8: Potato: Are the trends of increased global production sustainable. Food Secur 4:477–508. https://doi.org/10.1007/s12571-012-0220-1

Brown KW (1976) Sugar beet and potatoes. In: Monteith JL (ed) Vegetation and the Atmosphere, vol 2. London, Academic Press, pp 65–86

Brunsell NA, Wilson CJ (2013) Multiscale Interactions between Water and Carbon Fluxes and Environmental Variables in A Central U.S Grassland. Entropy 15:1324–1341. https://doi.org/10.3390/e15041324

Buysse P, Bodson B, Debacq A et al (2017) Carbon budget measurement over 12 years at a crop production site in the silty-loam region in Belgium. Agric for Meteorol 246:241–255. https://doi.org/10.1016/j.agrformet.2017.07.004

Cabral OMR, Rocha HR, Gash JH et al (2013) Fluxes of CO_2 above a sugarcane plantation in Brazil. Agric Meteorol 182–183:54–66. https://doi.org/10.1016/j.agrformet.2013.08.004

Chen S, Chen J, Lin G et al (2009) Energy balance and partition in Inner Mongolia steppe ecosystems with different land use types. Agric Meteorol 149:1800–1809. https://doi.org/10.1016/j.agrformet.2009.06.009

Ciais P, Reichstein M, Viovy N et al (2005) Europe-wide reduction in primary productivity caused by the heat and drought in 2003. Nature 437:529–533. https://doi.org/10.1038/nature03972

De Kauwe MG, Medlyn BE, Knauer J, Williams CA (2017) Ideas and perspectives: How coupled is the vegetation to the boundary layer? Biogeosciences 14:4435–4453. https://doi.org/10.5194/bg-14-4435-2017

De La Motte LG, Beauclaire Q, Heinesch B et al (2020) Non-stomatal processes reduce gross primary productivity in temperate forest ecosystems during severe edaphic drought: Edaphic drought in forest ecosystems. Philos Trans R Soc B Biol Sci 375. https://doi.org/10.1098/rstb.2019.0527

Devaux A, Kromann P, Ortiz O (2014) Potatoes for Sustainable Global Food Security. Potato Res 57:185–199. https://doi.org/10.1007/s11540-014-9265-1

Díaz E, Adsuara JE, Martínez ÁM et al (2022) Inferring causal relations from observational long-term carbon and water fluxes records. Sci Rep 12:1–12. https://doi.org/10.1038/s41598-022-05377-7

Eamus D, Huete A, Yu Q (2016) Modelling radiation exchange and energy balances of leaves and canopies. In: Vegetation Dynamics: A Synthesis of Plant Ecophysiology, Remote Sensing and Modelling. Cambridge University Press, pp 244–259

Evans JR (2021) Mesophyll conductance: walls, membranes and spatial complexity. New Phytol 229:1864–1876. https://doi.org/10.1111/nph.16968

Evans JR, Poorter H (2001) Photosynthetic acclimation of plants to growth irradiance: The relative importance of specific leaf area and nitrogen partitioning in maximizing carbon gain. Plant Cell Environ 24:755–767. https://doi.org/10.1046/j.1365-3040.2001.00724.x

Falge E, Baldocchi D, Olson R et al (2001) Gap filling strategies for defensible annual sums of net ecosystem exchange. Agric Meteorol 107:43–69. https://doi.org/10.1016/S0168-1923(00)00225-2

Falge E, Baldocchi D, Tenhunen J et al (2002) Seasonality of ecosystem respiration and gross primary production as derived from FLUXNET measurements. Agric Meteorol 113:53–74. https://doi.org/10.1016/S0168-1923(02)00102-8

Fatichi S, Leuzinger S, Körner C (2014) Moving beyond photosynthesis: From carbon source to sink-driven vegetation modeling. New Phytol 201:1086–1095. https://doi.org/10.1111/nph.12614

Fei X, Jin Y, Zhang Y et al (2017) Eddy covariance and biometric measurements show that a savanna ecosystem in Southwest China is a carbon sink. Sci Rep 7:1–14. https://doi.org/10.1038/srep41025

Fereres E, Soriano MA (2007) Deficit irrigation for reducing agricultural water use. J Exp Bot 58:147–159. https://doi.org/10.1093/jxb/erl165

Ferreira MI (2017) Stress coefficients for soil water balance combined with water stress indicators for irrigation scheduling of woody crops. Horticulturae 3. https://doi.org/10.3390/horticulturae3020038

Field CB, Jackson RB, Mooney HA (1995) Stomatal responses to increased CO_2: implications from the plant to the global scale. Plant Cell Environ 18:1214–1225. https://doi.org/10.1111/j.1365-3040.1995.tb00630.x

Flexas J, Barbour MM, Brendel O et al (2012) Mesophyll diffusion conductance to CO_2: An unappreciated central player in photosynthesis. Plant Sci 193–194:70–84. https://doi.org/10.1016/j.plantsci.2012.05.009

Flexas J, Bota J, Loreto F et al (2004) Diffusive and metabolic limitations to photosynthesis under drought and salinity in C3 plants. Plant Biol 6:269–279. https://doi.org/10.1055/s-2004-820867

Flexas J, Medrano H (2002) Drought-inhibition of photosynthesis in C3 plants: Stomatal and non-stomatal limitations revisited. Ann Bot 89:183–189. https://doi.org/10.1093/aob/mcf027

Foken T, Leuning R, Oncley SR et al (2012) Corrections and data quality control. In: A Practical Guide to Measurement and Data Analysis. Springer ScienceCBusiness Media B.V. 2012, Bayreuth, Germany, pp 85–131

Galmés J, Medrano H, Flexas J (2007) Photosynthetic limitations in response to water stress and recovery in Mediterranean plants with different growth forms. New Phytol 175:81–93. https://doi.org/10.1111/j.1469-8137.2007.02087.x

Gentilesca T, Battipaglia G, Borghetti M et al (2021) Evaluating growth and intrinsic water-use efficiency in hardwood and conifer mixed plantations. Trees - Struct Funct 35:1329–1340. https://doi.org/10.1007/s00468-021-02120-z

Gentine P, Green JK, Guérin M et al (2019) Coupling between the terrestrial carbon and water cycles - A review. Environ Res Lett 14. https://doi.org/10.1088/1748-9326/ab22d6

Ghislain M, Núñez J, Herrera MDR, Spooner DM (2009) The single Andigenum origin of Neo-Tuberosum potato materials is not supported by microsatellite and plastid marker analyses. Theor Appl Genet 118:963–969. https://doi.org/10.1007/s00122-008-0953-6

Gondim PSDS, Lima JRDS, Antonino AC et al (2015) Environmental control on water vapour and energy exchanges over grasslands in

semiarid region of brazil. Rev Bras Eng Agric e Ambient 19:3–8. https://doi.org/10.1590/1807-1929/agriambi.v19n1p3-8
Gonzalez-Paleo L, Ravetta DA (2018) Relationship between photosynthetic rate, water use and leaf structure in desert annual and perennial forbs differing in their growth. Photosynthetica 56:1177–1187. https://doi.org/10.1007/s11099-018-0810-z
Goorman R, Bartual A, Paula S, Ojeda F (2011) Enhancement of photosynthesis in post-disturbance resprouts of two co-occurring Mediterranean Erica species. Plant Ecol 212:2023–2033. https://doi.org/10.1007/s11258-011-9967-2
Grossiord C, Gessler A, Granier A et al (2014) Interspecific competition influences the response of oak transpiration to increasing drought stress in a mixed Mediterranean forest. For Ecol Manage 318:54–61. https://doi.org/10.1016/j.foreco.2014.01.004
Guo R, Cy Z, Shi Y et al (2017) Low carbon development and local sustainability from a carbon balance perspective. Resour Conserv Recycl 122:270–279. https://doi.org/10.1016/j.resconrec.2017.02.019
Haiqiang G, Bin Z, Jiquan C et al (2010) Seasonal changes of energy fluxes in an estuarine wetland of Shanghai, China. Chinese Geogr Sci 20:023–029. https://doi.org/10.1007/s11769-010-0023-2
Herbst M, Kutsch WL, Hummelshøj P et al (2002) Canopy physiology: interpreting the variations in eddy fluxes of water vapour and carbon dioxide observed over a beech forest. Basic Appl Ecol 3:157–169. https://doi.org/10.1078/1439-1791-00093
Hill D, Nelson D, Hammond J, Bell L (2021) Morphophysiology of Potato (*Solanum tuberosum*) in Response to Drought Stress: Paving the Way Forward. Front Plant Sci 11:1–19. https://doi.org/10.3389/fpls.2020.597554
Hu Z, Yu G, Fu Y et al (2008) Effects of vegetation control on ecosystem water use efficiency within and among four grassland ecosystems in China. Glob Chang Biol 14:1609–1619. https://doi.org/10.1111/j.1365-2486.2008.01582.x
Hunt R (1990) Basic growth analysis. Plant growth analysis for beginners. London, Unwin, Hyman, Boston, Sydney and Wellington. https://doi.org/10.1007/978-94-010-9117-6
Irmak S, Mutiibwa D (2010) On the dynamics of canopy resistance: Generalized linear estimation and relationships with primary micrometeorological variables. Water Resour Res 46:1–20. https://doi.org/10.1029/2009WR008484
Jarvis PG (1985) Jarvis 1985.pdf
Jarvis PG, Mcnaughton KG (1986) Stomatal Control of Transpiration: Scaling Up from Leaf to Region. Adv Ecol Res 15:1–49. https://doi.org/10.1016/S0065-2504(08)60119-1
Jia X, Zha TS, Wu B et al (2014) Biophysical controls on net ecosystem CO_2 exchange over a semiarid shrubland in northwest China. Biogeosciences 11:4679–4693. https://doi.org/10.5194/bg-11-4679-2014
Jongen M, Pereira JS, Aires LMI, Pio CA (2011) The effects of drought and timing of precipitation on the inter-annual variation in ecosystem-atmosphere exchange in a Mediterranean grassland. Agric for Meteorol 151:595–606. https://doi.org/10.1016/j.agrformet.2011.01.008
Jullien A, Allirand JM, Mathieu A et al (2009) Variations in leaf mass per area according to N nutrition, plant age, and leaf position reflect ontogenetic plasticity in winter oilseed rape (Brassica napus L.). F Crop Res 114:188–197. https://doi.org/10.1016/j.fcr.2009.07.015
Kang M, Zhang Z, Noormets A et al (2015) Energy partitioning and surface resistance of a poplar plantation in northern China. Biogeosciences 12:4245–4259. https://doi.org/10.5194/bg-12-4245-2015
Katul G, Manzoni S, Palmroth S, Oren R (2010) A stomatal optimization theory to describe the effects of atmospheric CO_2 on leaf photosynthesis and transpiration. Ann Bot 105:431–442. https://doi.org/10.1093/aob/mcp292
Katul GG, Palmroth S, Oren R (2009) Leaf stomatal responses to vapour pressure deficit under current and CO_2-enriched atmosphere explained by the economics of gas exchange. Plant Cell Environ 32:968–979. https://doi.org/10.1111/j.1365-3040.2009.01977.x
Keenan TF, Hollinger DY, Bohrer G et al (2013) Increase in forest water-use efficiency as atmospheric carbon dioxide concentrations rise. Nature 499:324–327. https://doi.org/10.1038/nature12291
Kjelgaard JF, Stockle C (2001) Evaluating surface resistance for estimating corn and potato evapotranspiration with the Penman-Monteith model. Trans Am Soc Agric Eng 44:797–805. https://doi.org/10.13031/2013.6243
Krich C, Mahecha MD, Migliavacca M et al (2022) Decoupling between ecosystem photosynthesis and transpiration. Environ Res Lett 17:22. https://doi.org/10.1088/1748-9326/ac583e
Kumagai T, Tateishi M, Shimizu T, Otsuki K (2008) Transpiration and canopy conductance at two slope positions in a Japanese cedar forest watershed. Agric for Meteorol 148:1444–1455. https://doi.org/10.1016/j.agrformet.2008.04.010
Launiainen S, Katul GG, Kolari P et al (2011) Empirical and optimal stomatal controls on leaf and ecosystem level CO_2 and H_2O exchange rates. Agric for Meteorol 151:1672–1689. https://doi.org/10.1016/j.agrformet.2011.07.001
Law BE, Falge E, Gu L et al (2002) Environmental controls over carbon dioxide and water vapor exchange of terrestrial vegetation. Agric for Meteorol 113:97–120. https://doi.org/10.1016/S0168-1923(02)00104-1
Law BE, Williams M, Anthoni PM et al (2000) Measuring and modelling seasonal variation of carbon dioxide and water vapour exchange of a Pinus ponderosa forest subject to soil water deficit. Glob Chang Biol 6:613–630. https://doi.org/10.1046/j.1365-2486.2000.00339.x
Leonardi S, Gentilesca T, Guerrieri R et al (2012) Assessing the effects of nitrogen deposition and climate on carbon isotope discrimination and intrinsic water-use efficiency of angiosperm and conifer trees under rising CO 2 conditions. Glob Chang Biol 18:2925–2944. https://doi.org/10.1111/j.1365-2486.2012.02757.x
Leuning R (1995) A critical appraisal of combine stomatal model C3 plants. Plant Cell Environ 18:339–355
Li D, Fang K, Li Y et al (2017) Climate, intrinsic water-use efficiency and tree growth over the past 150 years in humid subtropical China. PLoS ONE 12:1–19. https://doi.org/10.1371/journal.pone.0172045
Li SG, Lai CT, Lee G et al (2005) Evapotranspiration from a wet temperate grassland and its sensitivity to microenvironmental variables. Hydrol Process 19:517–532. https://doi.org/10.1002/hyp.5673
Li Y, Zhang X, Shao Q et al (2022) Community Composition and Structure Affect Ecosystem and Canopy Water Use Efficiency Across Three Typical Alpine Ecosystems. Front Plant Sci 12:1–14. https://doi.org/10.3389/fpls.2021.771424
Lin BS, Lei H, Hu MC et al (2020) Canopy Resistance and Estimation of Evapotranspiration above a Humid Cypress Forest. Adv Meteorol 2020. https://doi.org/10.1155/2020/4232138
Lin YS, Medlyn BE, Duursma RA et al (2015) Optimal stomatal behaviour around the world. Nat Clim Chang 5:459–464. https://doi.org/10.1038/nclimate2550
Linderson ML, Mikkelsen TN, Ibrom A et al (2012) Up-scaling of water use efficiency from leaf to canopy as based on leaf gas exchange relationships and the modeled in-canopy light distribution. Agric for Meteorol 152:201–211. https://doi.org/10.1016/j.agrformet.2011.09.019
Liu X, Wang P, Song H, Zeng X (2021) Determinants of net primary productivity: Low-carbon development from the perspective of carbon sequestration. Technol Forecast Soc Change 172:121006. https://doi.org/10.1016/j.techfore.2021.121006

Loader NJ, Walsh RPD, Robertson I et al (2011) Recent trends in the intrinsic water-use efficiency of ringless rainforest trees in Borneo. Philos Trans R Soc B Biol Sci 366:3330–3339. https://doi.org/10.1098/rstb.2011.0037

Lombardozzi D, Levis S, Bonan G, Sparks JP (2012) Predicting photosynthesis and transpiration responses to ozone: Decoupling modeled photosynthesis and stomatal conductance. Biogeosciences 9:3113–3130. https://doi.org/10.5194/bg-9-3113-2012

López-Olivari R, Fuentes S, Poblete-Echeverría C et al (2022) Site-Specific Evaluation of Canopy Resistance Models for Estimating Evapotranspiration over a Drip-Irrigated Potato Crop in Southern Chile under Water-Limited Conditions. Water (Switzerland) 14. https://doi.org/10.3390/w14132041

Mallick K, Trebs I, Boegh E et al (2016) Canopy-scale biophysical controls of transpiration and evaporation in the Amazon Basin. Hydrol Earth Syst Sci 20:4237–4264. https://doi.org/10.5194/hess-20-4237-2016

Martínez-Maldonado FE, Castaño-Marin AM, Góez-Vinasco GA, Marin FR (2021) Gross Primary Production of Rainfed and Irrigated Potato (*Solanum tuberosum L.*) in the Colombian Andean Region Using Eddy Covariance Technique. Water 13:15. https://doi.org/10.3390/w13223223

Martinez Maldonado FE, Marin FR (2023) Analytical approach to relate evapotranspiration, canopy-atmosphere coupling level, and water deficit sensitivity. Bragantia 82:1–14. https://doi.org/10.1590/1678-4499.20220198

McNaughton KG, Jarvis PG (1991) Effects of spatial scale on stomatal control of transpiration. Agric for Meteorol 54:279–302. https://doi.org/10.1016/0168-1923(91)90010-N

Meshalkina JL, Yaroslavtsev AM, Vasenev II et al (2018) Carbon balance assessment by eddy covariance method for agroecosystems with potato plants and oats & vetch mixture on sod-podzolic soils of Russia. IOP Conf Ser Earth Environ Sci 107. https://doi.org/10.1088/1755-1315/107/1/012119

Meshalkina JL, Yaroslavtsev AM, Vasenev II et al (2018) Carbon balance assessment by eddy covariance method for agroecosystems with potato plants and oats & vetch mixture on sod-podzolic soils of Russia. IOP Conf Ser Earth Environ Sci 107. https://doi.org/10.1088/1755-1315/107/1/012119

Migliavacca M, Meroni M, Manca G et al (2009) Seasonal and interannual patterns of carbon and water fluxes of a poplar plantation under peculiar eco-climatic conditions. Agric for Meteorol 149:1460–1476. https://doi.org/10.1016/j.agrformet.2009.04.003

Monteith J, Unsworth M (2013) Principles of environmental physics: Plants, animals, and the atmosphere: Fourth Edition, Fourth. Oxford, UK

Moors EJ, Jacobs C, Jans W et al (2010) Variability in carbon exchange of European croplands. Agric Ecosyst Environ 139:325–335. https://doi.org/10.1016/j.agee.2010.04.013

Morén AS, Lindroth A, Grelle A (2001) Water-use efficiency as a means of modelling net assimilation in boreal forests. Trees - Struct Funct 15:67–74. https://doi.org/10.1007/s004680000078

Mosquera Vásquez T, Del Castillo S, Gálvez DC, Rodríguez LE (2017) Breeding Differently: Participatory Selection and Scaling Up Innovations in Colombia. Potato Res 60:361–381. https://doi.org/10.1007/s11540-018-9389-9

Nadal-Sala D, Grote R, Birami B et al (2021) Leaf Shedding and Non-Stomatal Limitations of Photosynthesis Mitigate Hydraulic Conductance Losses in Scots Pine Saplings During Severe Drought Stress. Front Plant Sci 12. https://doi.org/10.3389/fpls.2021.715127

Nassif DSP, Marin FR, Costa LG (2014) Evapotranspiration and Transpiration Coupling to the Atmosphere of Sugarcane in Southern Brazil: Scaling Up from Leaf to Field. Sugar Tech 16:250–254. https://doi.org/10.1007/s12355-013-0267-0

Nelson JA, Carvalhais N, Migliavacca M et al (2018) Water-stress-induced breakdown of carbon-water relations: Indicators from diurnal FLUXNET patterns. Biogeosciences 15:2433–2447. https://doi.org/10.5194/bg-15-2433-2018

Niinemets Ü, Cescatti A, Rodeghiero M, Tosens T (2006) Complex adjustments of photosynthetic potentials and internal diffusion conductance to current and previous light availabilities and leaf age in Mediterranean evergreen species Quercus ilex. Plant Cell Environ 29:1159–1178. https://doi.org/10.1111/j.1365-3040.2006.01499.x

Niu S, Xing X, Zhang Z et al (2011) Water-use efficiency in response to climate change: From leaf to ecosystem in a temperate steppe. Glob Chang Biol 17:1073–1082. https://doi.org/10.1111/j.1365-2486.2010.02280.x

Obidiegwu JE, Bryan GJ, Jones HG, Prashar A (2015) Coping with drought: Stress and adaptive responses in potato and perspectives for improvement. Front Plant Sci 6:1–23. https://doi.org/10.3389/fpls.2015.00542

Oo AZ, Yamamoto A, Ono K et al (2023) Ecosystem carbon dioxide exchange and water use efficiency in a triple-cropping rice paddy in Southern India: A two-year field observation. Sci Total Environ 854:158541. https://doi.org/10.1016/j.scitotenv.2022.158541

Pereira JS, Mateus JA, Aires LM et al (2007) Net ecosystem carbon exchange in three contrasting Mediterranean ecosystems - The effect of drought. Biogeosciences 4:791–802. https://doi.org/10.5194/bg-4-791-2007

Perez PJ, Lecina S, Castellvi F et al (2006) A simple parameterization of bulk canopy resistance from climatic variables for estimating hourly evapotranspiration. Hydrol Process 20:515–532. https://doi.org/10.1002/hyp.5919

Raker CM, Spooner DM, Hawkes B (2002) The Andean populations: Microsatellite data. This study tests the genetic difference between landrace popula-. Crop Sci 1458:1451–1458. https://doi.org/10.2135/cropsci2002.1451

Rana G, Ferrara RM, Vitale D et al (2016) Carbon assimilation and water use efficiency of a perennial bioenergy crop (Cynara cardunculus L.) in Mediterranean environment. Agric for Meteorol 217:137–150. https://doi.org/10.1016/j.agrformet.2015.11.025

Rana G, Katerji N, Mastrorilli M, El Moujabber M (1994) Evapotranspiration and canopy resistance of grass in a Mediterranean region. Theor Appl Climatol 50:61–71. https://doi.org/10.1007/BF00864903

Reichstein M, Tenhunen JD, Roupsard O et al (2002) Severe drought effects on ecosystem CO_2 and H_2O fluxes at three Mediterranean evergreen sites: Revision of current hypotheses? Glob Chang Biol 8:999–1017. https://doi.org/10.1046/j.1365-2486.2002.00530.x

Samanta S, Banerjee S, Mukherjee A et al (2020) Determining the radiation use efficiency of potato using sunshine hour data: A simple and costless approach. Spanish J Agric Res 18:1–15. https://doi.org/10.5424/sjar/2020182-15561

Schwalm CR, Williams CA, Schaefer K et al (2010) Assimilation exceeds respiration sensitivity to drought: A FLUXNET synthesis. Glob Chang Biol 16:657–670. https://doi.org/10.1111/j.1365-2486.2009.01991.x

Scott RL, Huxman TE, Cable WL, Emmerich WE (2006) Partitioning of evapotranspiration and its relation to carbon dioxide exchange in a Chihuahuan Desert shrubland. Hydrol Process 20:3227–3243. https://doi.org/10.1002/hyp.6329

Shao J, Zhou X, Luo Y et al (2015) Biotic and climatic controls on interannual variability in carbon fluxes across terrestrial ecosystems. Agric for Meteorol 205:11–22. https://doi.org/10.1016/j.agrformet.2015.02.007

da Silva PF, de Sousa Lima JR, Antonino ACD et al (2017) Seasonal patterns of carbon dioxide, water and energy fluxes over the Caatinga and grassland in the semi-arid region of Brazil. J Arid

Environ 147:71–82. https://doi.org/10.1016/j.jaridenv.2017.09.003
Soil Survey Staff (2014) Keys to soil taxonomy, 12th edn. USDA-Natural Resources Conservation Service, Washington DC, EE.UU
Souza PJDOPD, Ribeiro A, Rocha EJPD et al (2012) Sazonalidade no balanço de energia em áreas de cultivo de soja na Amazônia. Bragantia 71:548–557. https://doi.org/10.1590/s0006-87052012000400013
Spinelli GM, Snyder RL, Sanden BL et al (2018) Low and variable atmospheric coupling in irrigated Almond (Prunus dulcis) canopies indicates a limited influence of stomata on orchard evapotranspiration. Agric Water Manag 196:57–65. https://doi.org/10.1016/j.agwat.2017.10.019
Spinelli GM, Snyder RL, Sanden BL, Shackel KA (2016) Water stress causes stomatal closure but does not reduce canopy evapotranspiration in almond. Agric Water Manag 168:11–22. https://doi.org/10.1016/j.agwat.2016.01.005
Steduto P, Hsiao TC (1998) Maize canopies under two soil water regimes III. Variation in coupling with the atmosphere and the role of leaf area index. Agric for Meteorol 89:201–213. https://doi.org/10.1016/S0168-1923(97)00083-X
Sugiura D, Terashima I, Evans JR (2020) A decrease in mesophyll conductance by Cell-Wall thickening contributes to photosynthetic downregulation. Plant Physiol 183:1600–1611. https://doi.org/10.1104/pp.20.00328
Sutherlin CE, Brunsell NA, de Oliveira G et al (2019) Contrasting physiological and environmental controls of evapotranspiration over Kernza Perennial crop, annual crops, and C4 and mixed C3/C4 grasslands. Sustain 11. https://doi.org/10.3390/su11061640
Tagesson T, Fensholt R, Cropley F et al (2015) Dynamics in carbon exchange fluxes for a grazed semi-arid savanna ecosystem in West Africa. Agric Ecosyst Environ 205:15–24. https://doi.org/10.1016/j.agee.2015.02.017
Tang J, Bolstad P V, Ewers BE et al (2006) Sap flux-upscaled canopy transpiration, stomatal conductance, and water use efficiency in an old growth forest in the Great Lakes region of the United States. J Geophys Res Biogeosciences 111. https://doi.org/10.1029/2005JG000083
Tang X, Ding Z, Li H et al (2015) Characterizing ecosystem water-use efficiency of croplands with eddy covariance measurements and MODIS products. Ecol Eng 85:212–217. https://doi.org/10.1016/j.ecoleng.2015.09.078
de Castro Teixeira AH, Bastiaanssen WG, Ahmad MUD et al (2008) Analysis of energy fluxes and vegetation-atmosphere parameters in irrigated and natural ecosystems of semi-arid Brazil. J Hydrol 362:110–127. https://doi.org/10.1016/j.jhydrol.2008.08.011
Vadez V, Kholova J, Medina S et al (2014) Transpiration efficiency: New insights into an old story. J Exp Bot 65:6141–6153. https://doi.org/10.1093/jxb/eru040
Van Dijke AJH, Mallick K, Schlerf M et al (2020) Examining the link between vegetation leaf area and land-atmosphere exchange of water, energy, and carbon fluxes using FLUXNET data. Biogeosciences 17:4443–4457. https://doi.org/10.5194/bg-17-4443-2020
Varone L, Ribas-Carbo M, Cardona C et al (2012) Stomatal and non-stomatal limitations to photosynthesis in seedlings and saplings of Mediterranean species pre-conditioned and aged in nurseries: Different response to water stress. Environ Exp Bot 75:235–247. https://doi.org/10.1016/j.envexpbot.2011.07.007
Wagle P, Xiao X, Kolb TE et al (2016) Differential responses of carbon and water vapor fluxes to climate among evergreen needleleaf forests in the USA. Ecol Process 5. https://doi.org/10.1186/s13717-016-0053-5
Waldo S, Chi J, Pressley SN et al (2016) Assessing carbon dynamics at high and low rainfall agricultural sites in the inland Pacific Northwest US using the eddy covariance method. Agric For Meteorol 218–219:25–36. https://doi.org/10.1016/j.agrformet.2015.11.018
Wehr R, Saleska SR (2021) Calculating canopy stomatal conductance from eddy covariance measurements, in light of the energy budget closure problem. Biogeosciences 18:13–24. https://doi.org/10.5194/bg-18-13-2021
Weraduwage SM, Chen J, Anozie FC et al (2015) The relationship between leaf area growth and biomass accumulation in Arabidopsis thaliana. Front Plant Sci 6:1–21. https://doi.org/10.3389/fpls.2015.00167
Wilson KB, Baldocchi DD, Hanson PJ (2001) Leaf age affects the seasonal pattern of photosynthetic capacity and net ecosystem exchange of carbon in a deciduous forest. Plant Cell Environ 24:571–583. https://doi.org/10.1046/j.0016-8025.2001.00706.x
Wood DA (2021) Net ecosystem carbon exchange prediction and insightful data mining with an optimized data-matching algorithm. Ecol Indic 124:107426. https://doi.org/10.1016/j.ecolind.2021.107426
Wright GC, Rao RCN, Farquhar GD (1994) Water-use efficiency and carbon isotope discrimination in peanut under water deficit conditions. Crop Sci 34:92–97. https://doi.org/10.2135/cropsci1994.0011183X003400010016x
Xie J, Chen J, Sun G et al (2016) Ten-year variability in ecosystem water use efficiency in an oak-dominated temperate forest under a warming climate. Agric for Meteorol 218–219:209–217. https://doi.org/10.1016/j.agrformet.2015.12.059
Xu L, Baldocchi DD (2004) Seasonal variation in carbon dioxide exchange over a Mediterranean annual grassland in California. Agric for Meteorol 123:79–96. https://doi.org/10.1016/j.agrformet.2003.10.004
Yang J, Duursma RA, De Kauwe MG et al (2019) Incorporating non-stomatal limitation improves the performance of leaf and canopy models at high vapour pressure deficit. Tree Physiol 39:1961–1974. https://doi.org/10.1093/treephys/tpz103
Zhang Y, Zhao W, He J, Zhang K (2016) Energy exchange and evapotranspiration over irrigated seed maize agroecosystems in a desert-oasis region, northwest China. Agric for Meteorol 223:48–59. https://doi.org/10.1016/j.agrformet.2016.04.002
Zhou J, Zhang Z, Sun G et al (2013) Response of ecosystem carbon fluxes to drought events in a poplar plantation in Northern China. For Ecol Manage 300:33–42. https://doi.org/10.1016/j.foreco.2013.01.007
Zhou S, Bofu Y, Huang Y, Wang G (2014) Geophysical Research Letters. Geophys Res Lett 41:5005–5013. https://doi.org/10.1002/2014GL060741
Zhou S, Yu B, Huang Y, Wang G (2015) Daily underlying water use efficiency for AmeriFlux sites. J Geophys Res Biogeosciences 120:887–902. https://doi.org/10.1002/2015JG002947.Received